

14

ELECTRICAL

E  
N  
G  
-  
N  
E  
E  
R  
-  
N  
G

---

ENGINEERING EXPERIMENT STATION  
AUBURN UNIVERSITY  
AUBURN, ALABAMA

MULTIVARIABLE CONTROL THEORY APPLIED TO HIERARCHICAL  
ATTITUDE CONTROL FOR PLANETARY SPACECRAFT

PREPARED BY

GUIDANCE AND CONTROL STUDY GROUP


J. S. BOLAND, III, CO-PROJECT LEADER

D. W. RUSSELL, CO-PROJECT LEADER

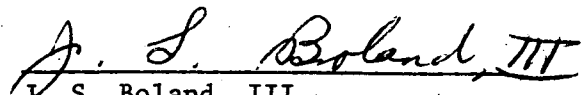
DECEMBER 8, 1972

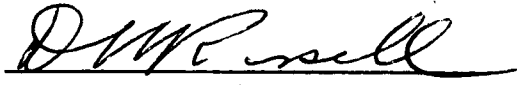
CONTRACT NAS8-27827  
GEORGE C. MARSHALL SPACE FLIGHT CENTER  
NATIONAL AERONAUTICS AND SPACE ADMINISTRATION  
HUNTSVILLE, ALABAMA

APPROVED BY:

  
\_\_\_\_\_  
M. A. Honnell  
Professor and Head (Acting)  
Electrical Engineering

SUBMITTED BY:

  
\_\_\_\_\_  
J. S. Boland, III  
Associate Professor  
Electrical Engineering

  
\_\_\_\_\_  
D. W. Russell  
Professor  
Electrical Engineering

## TABLE OF CONTENTS

FOREWORD	iii
SUMMARY	iv
PERSONNEL	v
LIST OF FIGURES	vi
LIST OF TABLES	vi
LIST OF SYMBOLS	viii
I. INTRODUCTION	1
II. THE REACTION CONTROL JET ATTITUDE CONTROL SYSTEM	6
III. THE CONTROL MOMENT GYRO ATTITUDE CONTROL SYSTEM	18
IV. COMBINED REACTION CONTROL JET AND CONTROL MOMENT GYRO ATTITUDE CONTROL SYSTEM	36
V. COMPUTATION OF DISTURBING TORQUES DUE TO MOTION OF TELEVISION CAMERA	41
VI. CONCLUSIONS AND RECOMMENDATIONS	52
REFERENCES	54
APPENDIX	55

## FOREWORD

This final report documents and summarizes the work accomplished by the Electrical Engineering Department, Auburn University, in the performance of Contract NAS8-27827 granted to Auburn University, Auburn, Alabama. The contract was awarded July 23, 1971, by the George C. Marshall Space Flight Center, National Aeronautics and Space Administration, Huntsville, Alabama.

## SUMMARY

This report applies multivariable control theory to the design of a hierarchical attitude control system for the CARD space vehicle. The system selected uses reaction control jets (RCJ) and control moment gyros (CMG). The RCJ system uses linear signal mixing and a no-fire region similar to that used on the Skylab program; the y-axis and z-axis systems which are coupled use a sum and difference feedback scheme. The CMG system uses the optimum steering law [4] and the same feedback signals as the RCJ system. When both systems are active the design is such that the torques from each system are never in opposition.

A state-space analysis was made of the CMG system to determine the general structure of the input matrices (steering law) and feedback matrices that will decouple the axes. It is shown that the optimum steering law and proportional-plus-rate feedback are special cases.

A third part of the report is a derivation of the disturbing torques on the space vehicle due to the motion of the on-board television camera. A simple procedure for computing an upper bound on these torques (given the system parameters) is included.

## PERSONNEL

The following staff members of Auburn University have actively participated in the work of this contract:

J. S. Boland, III - Associate Professor of Electrical Engineering

D. W. Russell - Professor of Electrical Engineering

W. G. Legg - Graduate Research Assistant in Electrical Engineering

## LIST OF FIGURES

I-1.	Baseline CARD Planetary Vehicle Concept . . . . .	3
I-2.	Baseline CARD Planetary Vehicle Concept . . . . .	4
I-3.	Baseline CARD Planetary Vehicle Concept . . . . .	5
II-1.	RCJ Attitude Control Thrusters . . . . .	7
II-2.	X-axis RCJ Attitude Control System . . . . .	8
II-3.	Y- and Z-axis RCJ Attitude Control System Block Diagram . . . . .	11
II-4.	Phase-plane Trajectories of RCJ System . . . . .	12
II-5.	Phase-plane Trajectories of RCJ System . . . . .	13
II-6.	Y-axis and Z-axis RCJ System Using Sum and Difference Saturation Signal . . . . .	14
II-7.	Boundaries of No-Fire Region for RCJ System Using Sum and Difference Saturation Signals . . . . .	15
II-8.	Phase-plane Trajectories of RCJ System - Sum and Difference Saturation Signals . . . . .	16
III-1.	CMG Cluster . . . . .	19
III-2.	CMG System Block Diagram . . . . .	20
III-3.	Block Diagram of Open-loop CMG System; Clamped Mode and Torque Motor Dynamics Neglected . . . . .	23
III-4.	Block Diagram of Open-loop CMG System; Clamped Mode and Torque Motor Dynamics Included . . . . .	29
III-5.	CMG Closed-loop System; Clamped Mode . . . . .	34
III-6.	CMG Closed-loop System with Proportional-plus-rate Feedback; Clamped Mode . . . . .	34
III-7.	Closed-loop System with Proportional-plus-rate Feedback; Clamped Mode . . . . .	35
III-8.	Closed-loop System with Proportional-plus-rate Feedback; Clamped Mode . . . . .	35

IV-1.	CMG System with Sum and Difference Saturation Signals . . . . .	37
IV-2.	Phase-plane Trajectory of Combined RCJ and CMG System . . . . .	38
IV-3.	Phase-plane Trajectories of Combined RCJ and CMG Systems . . . . .	39
IV-4.	Phase-plane Trajectories of Combined RCJ and CMG Systems . . . . .	40
V-1.	Television Camera and Mount . . . . .	42
V-2.	Television Camera Coordinates . . . . .	44
Table 1.	Disturbing Torques Due to Motion of Television Camera . . . . .	51



## LIST OF SYMBOLS

SYMBOL	DEFINITION
$A_{1x}$	X-axis rate feedback gain (RCJ System)
$A_{1y}$	Y-axis rate feedback gain (RCJ System)
$A_{1z}$	Z-axis rate feedback gain (RCJ System)
FDPX	X-axis feedback gain (see Fig. III-2)
FDPY	Y-axis feedback gain (see Fig. III-2)
FDPZ	Z-axis feedback gain (see Fig. III-2)
FPX	X-axis rate feedback gain (see Fig. III-2)
FPY	Y-axis rate feedback gain (see Fig. III-2)
FPZ	Z-axis rate feedback gain (see Fig. III-2)
$J_x$	Space vehicle X-axis moment-of-inertia
$J_y$	Space vehicle Y-axis moment-of-inertia
$J_z$	Space vehicle Z-axis moment-of-inertia
$M_{RX}$	X-axis reaction moment (see Fig. III-2)
$M_{RY}$	Y-axis reaction moment (see Fig. III-2)
$M_{RZ}$	Z-axis reaction moment (see Fig. III-2)
$M_x$	X-axis acceleration
$M_y$	Y-axis acceleration
$M_z$	Z-axis acceleration
MXCMND	X-axis command moment
MYCMND	Y-axis command moment
MZCMND	Z-axis command moment
$T_m$	Gyro torque-motor time constant

## SYMBOL

## DEFINITION

$T_x$	Disturbing torque about X-axis
$T_y$	Disturbing torque about Y-axis
$T_z$	Disturbing torque about Z-axis
$U_i$	Input variables
$X_i$	State variables
$Z_i$	State variables
$\delta_{ij}$	Gimbal angles (see Fig. III-1)
$\theta_c$	Rotation of TV camera about the Y-axis
$\phi_{cx}$	X-axis command input
$\phi_{cy}$	Y-axis command input
$\phi_{cz}$	Z-axis command input
$\phi_{db}$	Deadband
$\phi_R$	Saturation limit on feedback signals
$\phi_x$	Space vehicle rotation about the X-axis
$\phi_y$	Space vehicle rotation about the Y-axis
$\phi_z$	Space vehicle rotation about the Z-axis
$\psi_c$	Rotation of TV camera about the $Z_c$ -axis

## I. INTRODUCTION

The attitude control of a spacecraft visiting comets and asteroids for scientific study requires a multivariable attitude control system. During the journey from earth to rendezvous with the target (comet or asteroid), the attitude control is provided by the thrust vector control (TVC) system, the propulsion being supplied by a solar electric system augmented by a chemical propulsion unit. When the spacecraft rendezvous with the target, the attitude control for station keeping, docking, and separation from the target requires more capability than the TVC system can provide.

The objective of this study was to design a highly reliable attitude control system for experiment pointing, station keeping, docking and separation from the target for the Comet and Asteroid Rendezvous and Docking (CARD) space vehicle [1]. Early in the study it was determined that a combination of a reaction control jet (RCJ) control system and a control moment gyro (CMG) control system properly mated would be a good approach. Such systems have been successfully used on other space vehicles although problem areas still exist [2].

The RCJ system is by nature an on-off linear control system and for small errors will limit cycle; energy to generate torques is from an ever-decreasing supply of pressurized gases. On the other hand the CMG system is a continuous non-linear control system using solar energy to maintain the spinning of the gyros. For small disturbances the CMG system can keep the attitude errors inside the RCJ system dead-

band. The RCJ system is available to desaturate the CMG system and to correct for large disturbances.

The design objectives given primary consideration were:

- (1) Minimize fuel consumption when the RCJ system is the only active system, and when both systems are active design the system so that the torques produced are never in opposition.
- (2) Minimize coupling between the three axes of the attitude control system.

The spacecraft's general appearance, size, configuration, inertias, etc., were taken from the Northrup Services, Inc., final report of its feasibility study [1]. Figures I-1, I-2, I-3 are taken from that report

An additional area of study included in this report concerns the disturbances on the spacecraft due to the motion of the scanning platform on which is mounted the television camera. A procedure to compute the disturbing torques as a function of the television camera inertias and scanning rates is included.

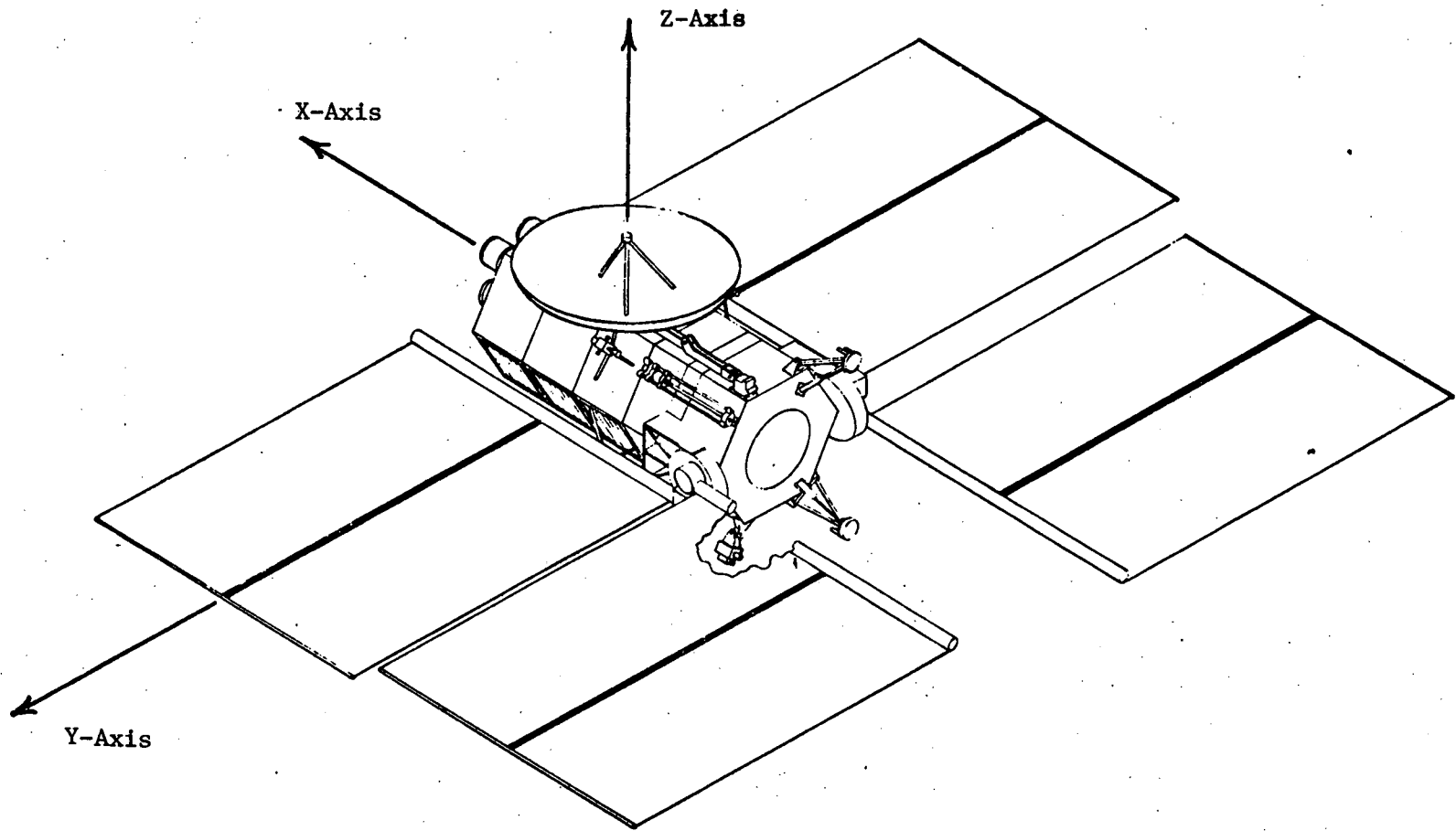


Figure I-1. Baseline CARD Planetary Vehicle Concept (from Ref 1)

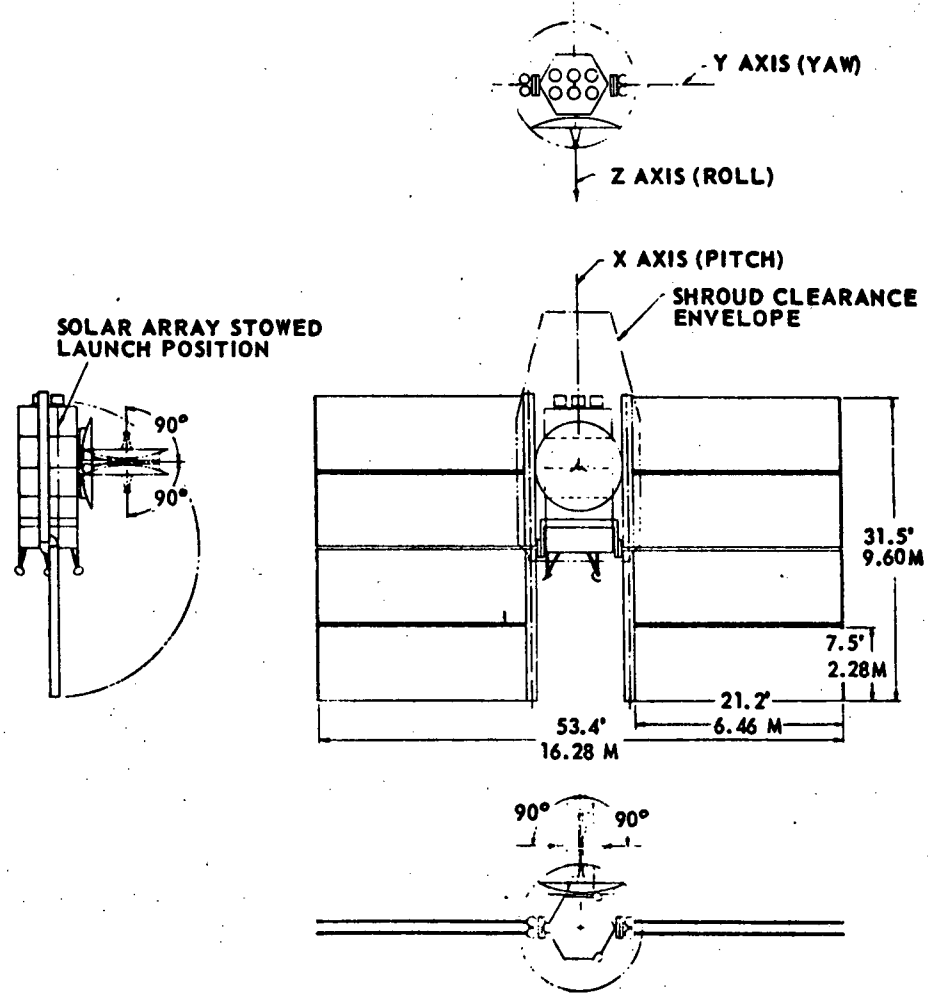


Figure I-2. Baseline CARD Planetary Vehicle Concept (from Ref 1)

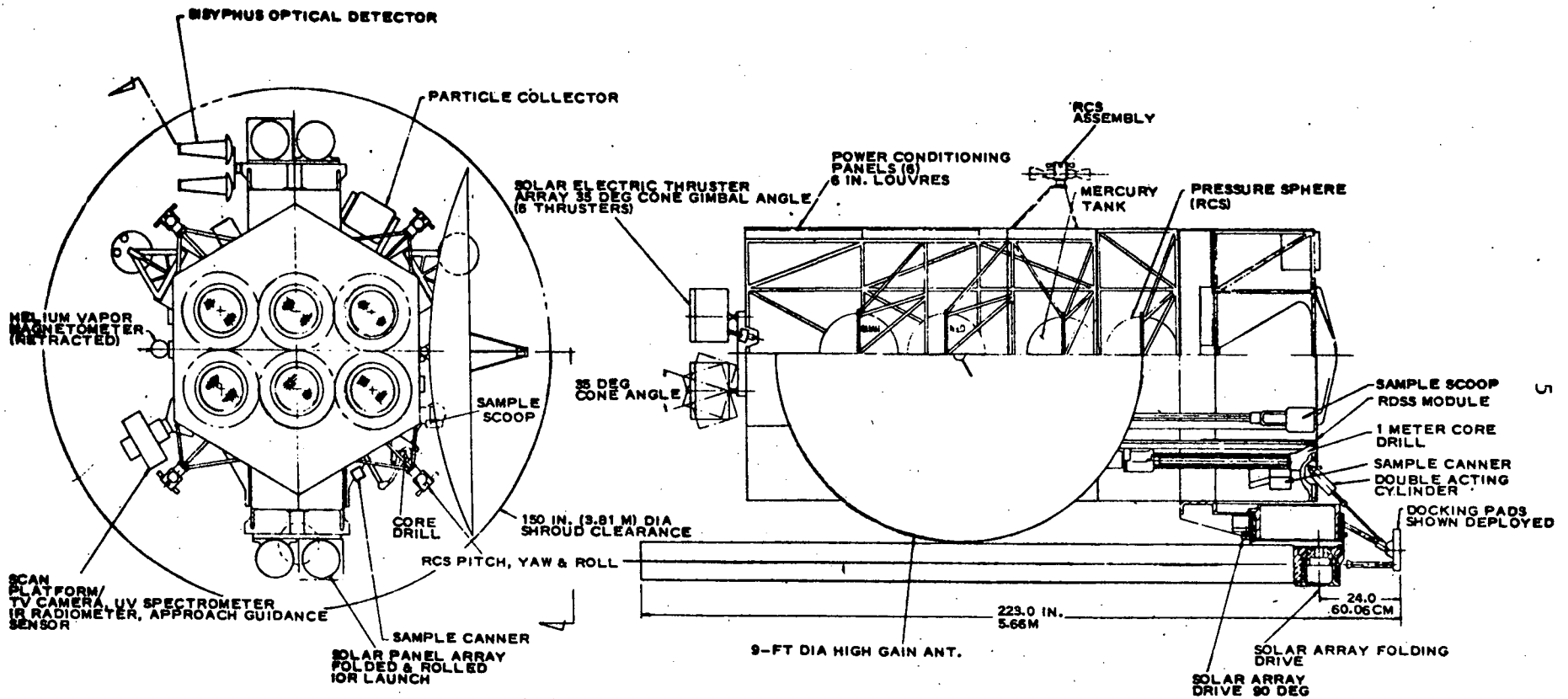


Figure I-3. Baseline CARD Planetary Vehicle Concept (from Ref 1)

## II. THE REACTION CONTROL JET ATTITUDE CONTROL SYSTEM

The attitude control system controls the orientation of the spacecraft with respect to the XYZ axes; the outputs are the angles  $\phi_x$ ,  $\phi_y$ ,  $\phi_z$ . The reaction control jet (RCJ) attitude control system uses cold gas thrusters to produce torques about the spacecraft center-of-gravity. The location of the thrusters is taken from [1]; the numbering of the thrusters and the spacecraft axes are as shown in Figure II-1. The spacecraft center-of-gravity is at the origin of the XYZ axes and it is assumed that the thrusters produce torques in the Y-Z plane.

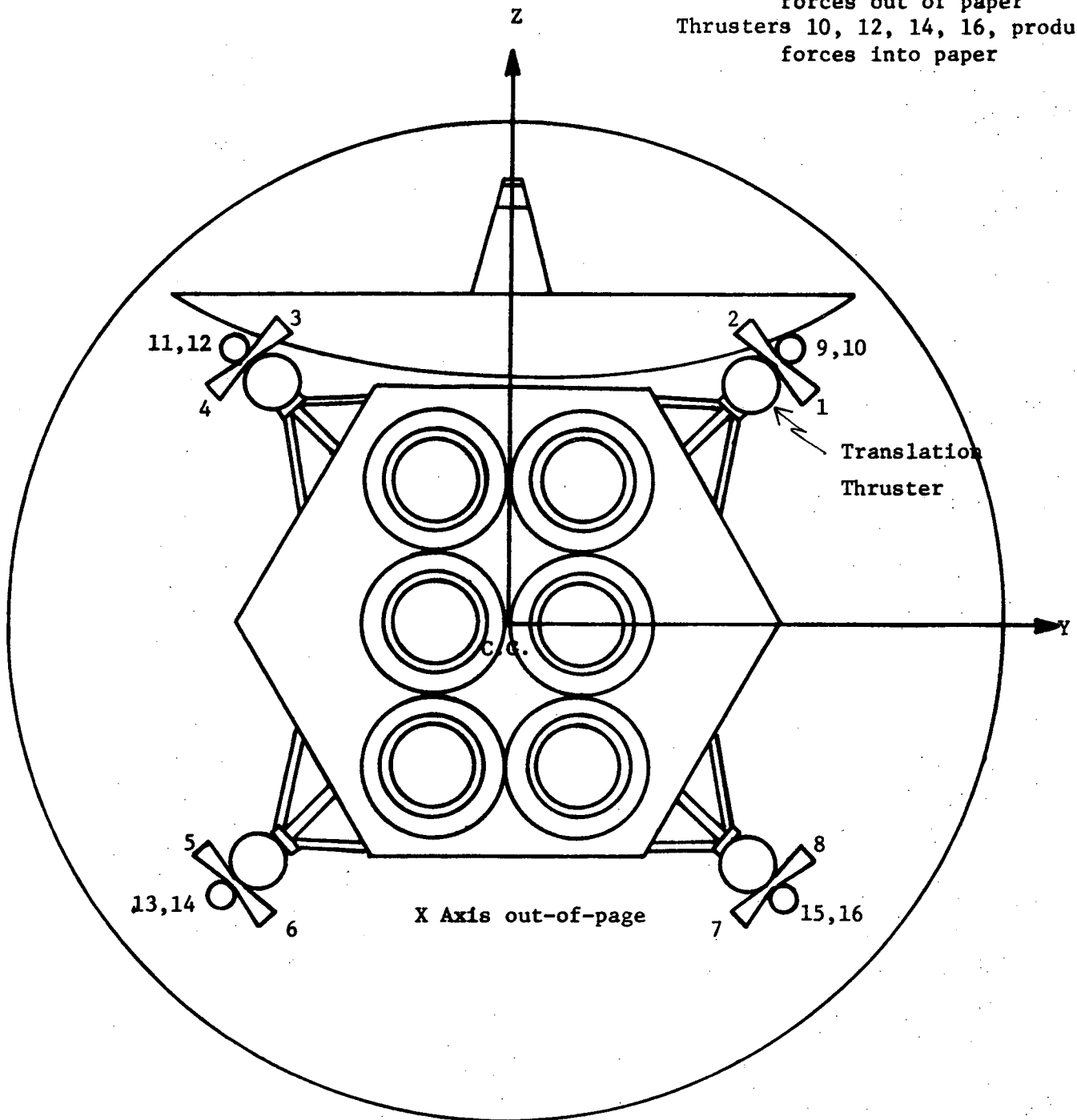
To simplify the analysis the dead-time, rise-time and decay-time of the thrusters are neglected; in addition it is assumed that all thrusters produce the same torque with no misalignment. Once an engine is activated it is assumed to continue to produce a constant torque for at least fifty milliseconds. This is a commonly used value.

The X-axis control system uses thrusters which produce no torques about the Y or Z axes. The control system uses proportional-plus-rate feedback with a saturation block in the position feedback path. This produces a no-fire region similar to that used in the Skylab program [2].

Figure II-2 contains a block diagram of the X-axis control system and a phase-plane showing the boundaries of the no-fire region. The controller parameters were calculated assuming that the system deadband,  $\phi_{db}$ , and the saturation value,  $\phi_R$ , were specified and that a trajectory originating on the rate limit boundary would intersect the  $\phi_x$  axis at  $\phi_{db}$ . The  $\phi_{db}$  specification represents a compromise between fuel consump-



Thrusters 9, 11, 13, 15 produce  
forces out of paper  
Thrusters 10, 12, 14, 16, produce  
forces into paper



NOTE: Attitude control thrusters are larger than scale  
to show numbering system.

Figure II-1. RCJ Attitude Control Thrusters

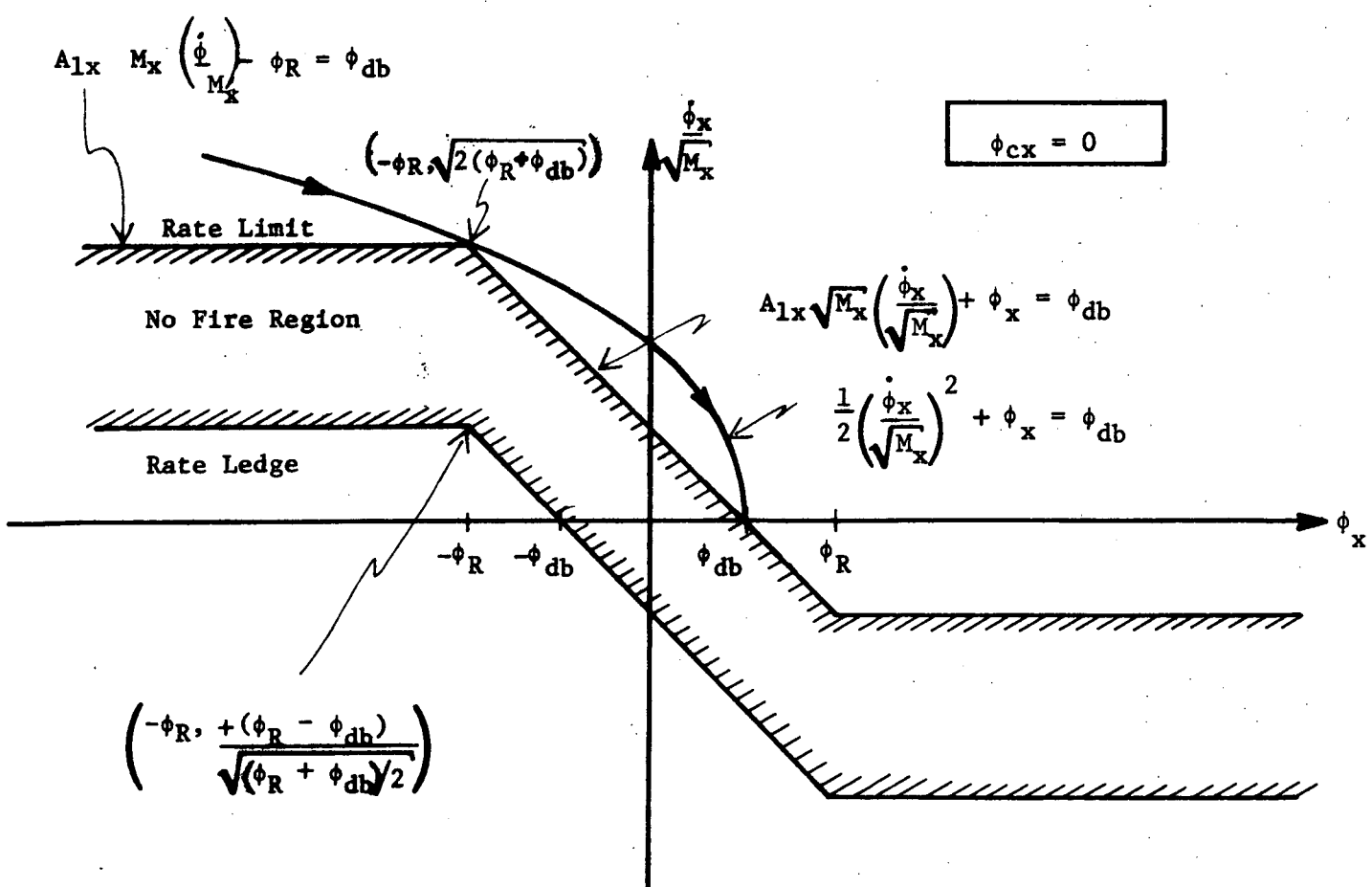
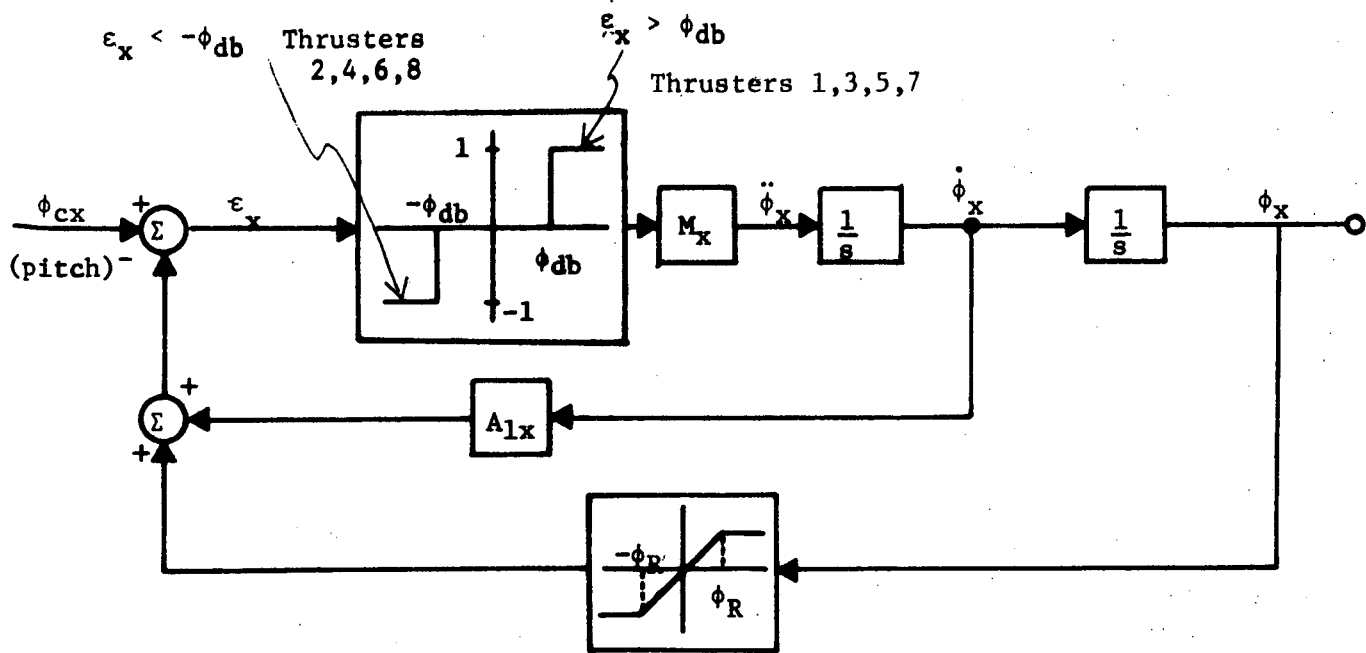


Figure II-2. X-axis RCJ Attitude Control System

tion and steady-state accuracy; the rate ledge specification represents a compromise between fuel consumption and speed of response.

$A_{1x}$  is computed in the following manner:

Assume  $\phi_c = 0$  and  $\epsilon_x < -\phi_{db}$  so that

$$\ddot{\phi}_x = \frac{d\dot{\phi}_x}{dt} = -M_x \quad (\text{II-1})$$

$$\text{Also } \frac{d\dot{\phi}_x}{dt} = \ddot{\phi}_x \quad (\text{II-2})$$

Dividing (II-2) by (II-1) yields

$$\frac{d\dot{\phi}_x}{\dot{\phi}_x} = -\frac{\dot{\phi}_x}{M_x}$$

or  $d\phi_x = -\frac{\dot{\phi}_x}{M_x} d\phi_x$

Integrating and requiring that the trajectory go through  $(\phi_{db}, 0)$  yields

$$\frac{1}{2} \left( \frac{\dot{\phi}_x}{\sqrt{M_x}} \right)^2 + \phi_x = \phi_{db} \quad (\text{II-3})$$

For  $-\phi_R \leq \phi_x \leq \phi_R$ , the boundary is given by

$$\epsilon_x = -\phi_{db} = -(A_{1x} \dot{\phi}_x + \phi_x) \quad (\text{II-4})$$

For the curves given by (II-3) and (II-4) to intersect at  $\phi_x = -\phi_R$  requires that

$$A_{1x} = \sqrt{\frac{\phi_R + \phi_{db}}{2M_x}} \quad (\text{II-5})$$

The rate ledge is 
$$\frac{(\phi_R - \phi_{db}) \sqrt{2}}{\sqrt{(\phi_R + \phi_{db})}}$$

Since the Y and Z axes share thrusters a linear-signal-mixing scheme [3] is used to insure that opposing thrusters are not energized at the same time. A block diagram of the system is shown in Figure II-3.  $A_{1Y}$  and  $A_{1Z}$  are calculated in the same manner as  $A_{1X}$ .

For the digital simulation the rate ledge is taken to be 0.172 degrees/second. From [1]  $\phi_{db} = 0.3^\circ$  and the acceleration produced in each axis, for error in that axis only, and the thrusters producing the acceleration are:

X axis: Solar panels rolled:  $\pm .208 \text{ deg/sec}^2$   
 (pitch) Solar panels extended:  $\pm .031 \text{ deg/sec}^2$   
 $+\ddot{\phi}_x$  produced by thrusters 1,3,5,7  
 $-\ddot{\phi}_x$  produced by thrusters 2,4,6,8

Y axis: Solar panels rolled:  $\pm .0391 \text{ deg/sec}^2$   
 (yaw) Solar panels extended:  $\pm .0214 \text{ deg/sec}^2$   
 $+\ddot{\phi}_y$  produced by thrusters 9, 11, 14, 16  
 $-\ddot{\phi}_y$  produced by thrusters 10, 12, 13, 15

Z axis: Solar panels rolled:  $\pm .0378 \text{ deg/sec}^2$   
 (roll) Solar panels extended:  $\pm .0126 \text{ deg/sec}^2$   
 $+\ddot{\phi}_z$  produced by thrusters 10, 11, 13, 16  
 $-\ddot{\phi}_z$  produced by thrusters 9, 12, 14, 15

Some typical trajectories are given in Figures II-4 and II-5.

A modification to this system was made which gives promise of better performance. In place of feeding the position signals  $\phi_y$  and  $\phi_z$  to the saturation blocks, the sum and difference,  $(\phi_y + \phi_z)$  and  $(\phi_z - \phi_y)$  are the inputs to the saturation blocks. The block diagram of this system is given in Figure II-6. Figure II-7 is a phase-plane plot showing the boundaries of the no-fire region. Figure II-8 is a typical trajectory for this system.

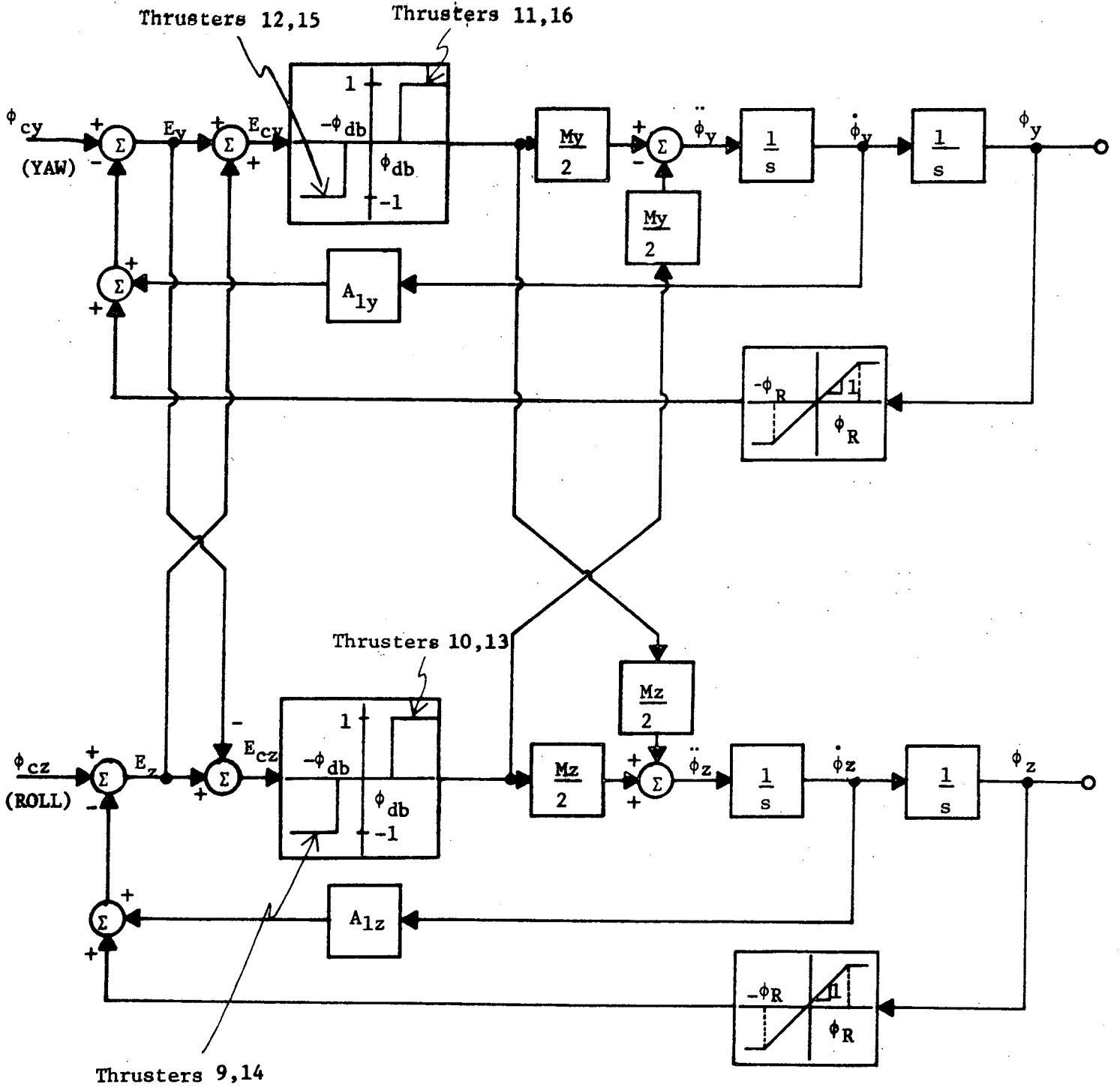
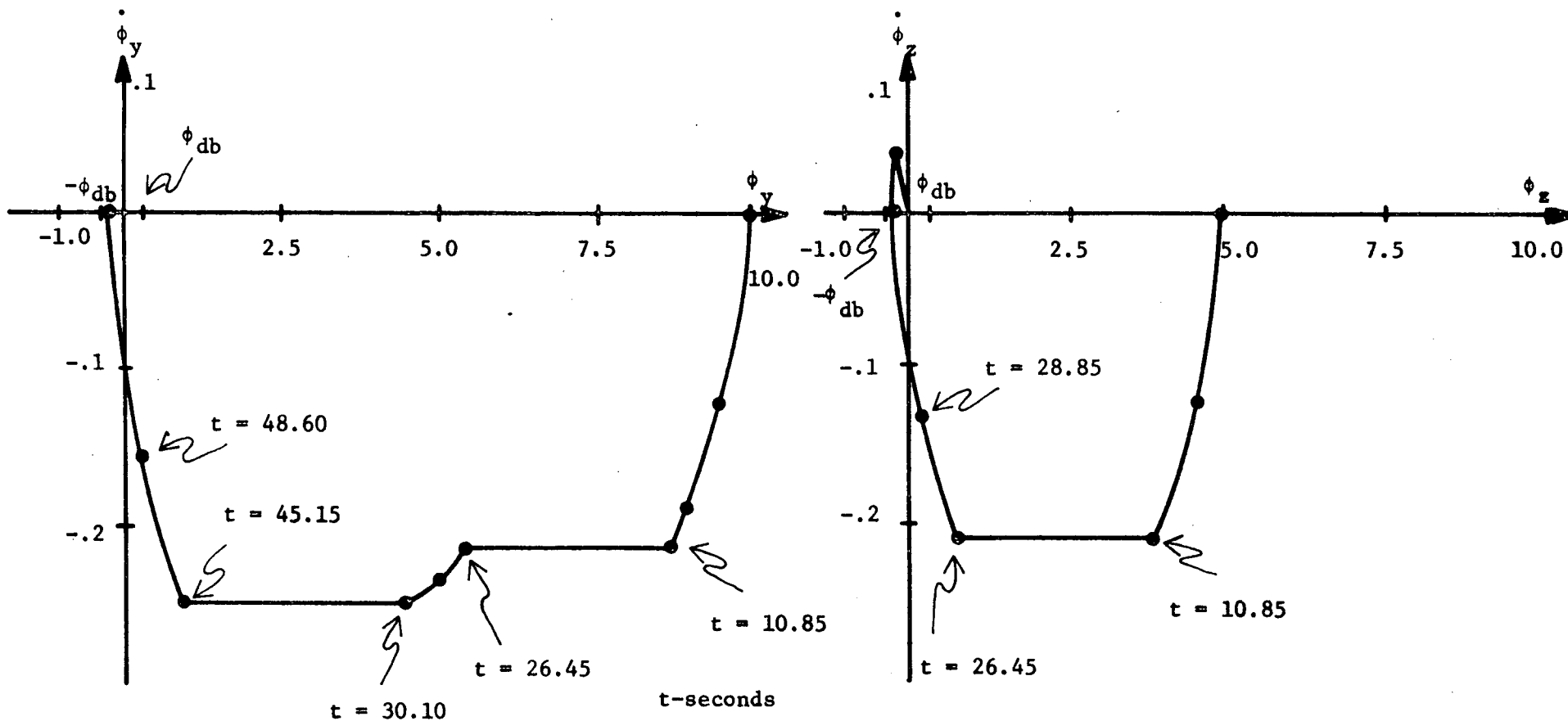


Figure II-3. Y-and-Z-axis RCJ Attitude Control System Block Diagram



INITIAL CONDITIONS

$\phi_{y0} = 10.0^\circ$   
 $\dot{\phi}_{y0} = 0.0^\circ/\text{sec.}$   
 $\phi_{z0} = 5.0^\circ$   
 $\dot{\phi}_{z0} = 0.0^\circ/\text{sec.}$

DESIGN PARAMETERS

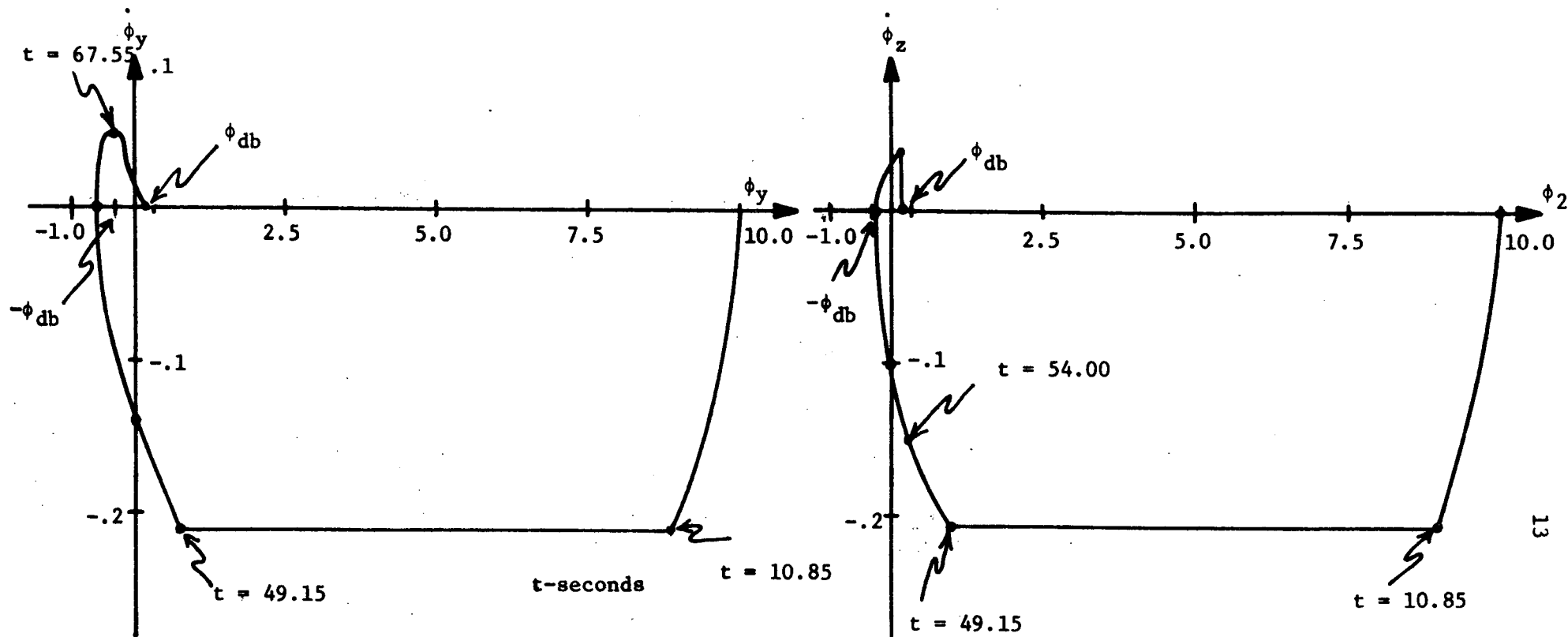
$\phi_{db} = \begin{matrix} + \\ - \end{matrix} .3^\circ$   
 $M_y = .0391$   
 $M_z = .0378$   
 $A_{1y} = 4.080$   
 $A_{1z} = 4.176$

RATE LEDGE = 0.172

RESULTS

- Time to reach and remain inside deadband:  
 $y - 48.60$  secs.  
 $z - 28.85$  secs.
- Fuel consumption at:  
 $48.60$  secs: 52.0  
 $28.85$  secs: 28.5  
 (1 unit is the energy consumed by one thruster firing for 1 sec.)

Figure II-4. Phase-plane Trajectories of RCJ System



INITIAL CONDITIONS

$\phi_{y0} = 10.0^\circ$   
 $\dot{\phi}_{y0} = 0.0^\circ/\text{sec}$   
 $\phi_{z0} = 10.0^\circ$   
 $\dot{\phi}_{z0} = 0.0^\circ/\text{sec}$

DESIGN PARAMETERS

$\phi_{db} = \pm .3^\circ$   
 $M_y = .0391$   
 $M_z = .0378$   
 $A_{1y} = 4.080$   
 $A_{1z} = 4.176$   
 RATE LEDGE = 0.172

RESULTS

1. Time to reach and remain inside deadband:
  - y - 67.55
  - z - 54.00
2. Fuel Consumption:
  - 67.55 sec: 49.1
  - 54.00 sec: 30.0
  - (1 unit is the energy consumed by 1 thruster firing for 1 sec)

Figure II - 5 Phase-plane Trajectories of RCJ System

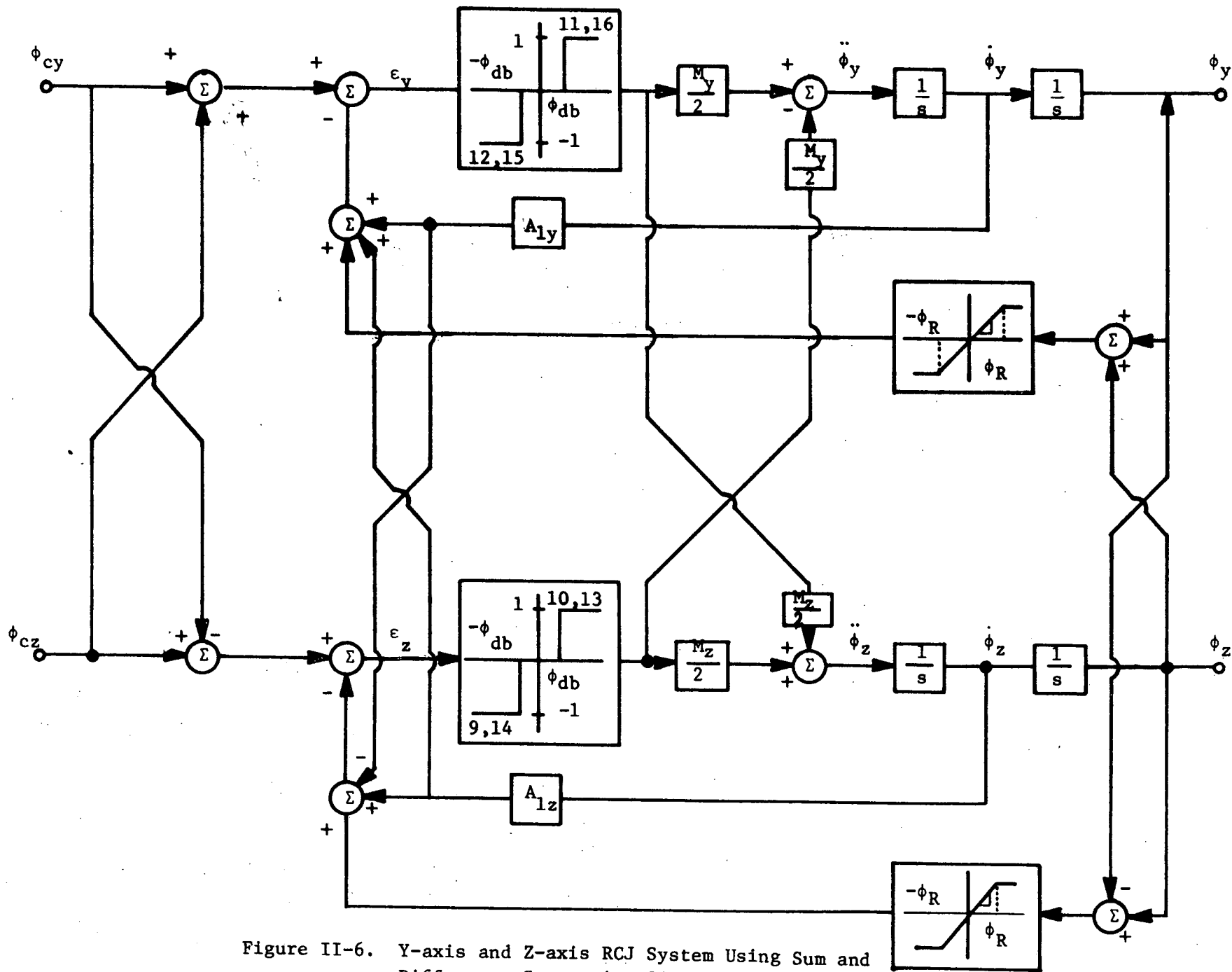


Figure II-6. Y-axis and Z-axis RCJ System Using Sum and Difference Saturation Signal



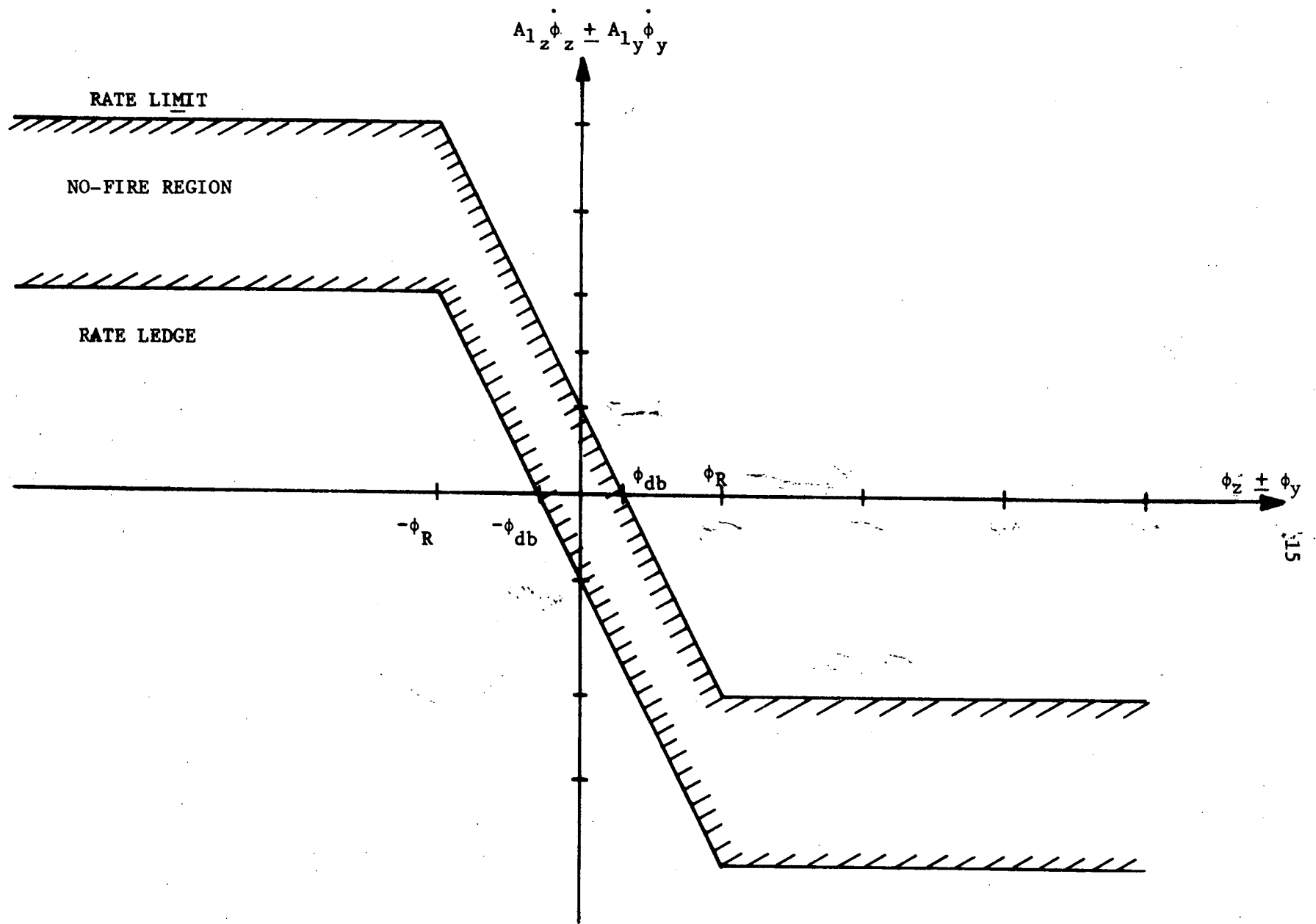
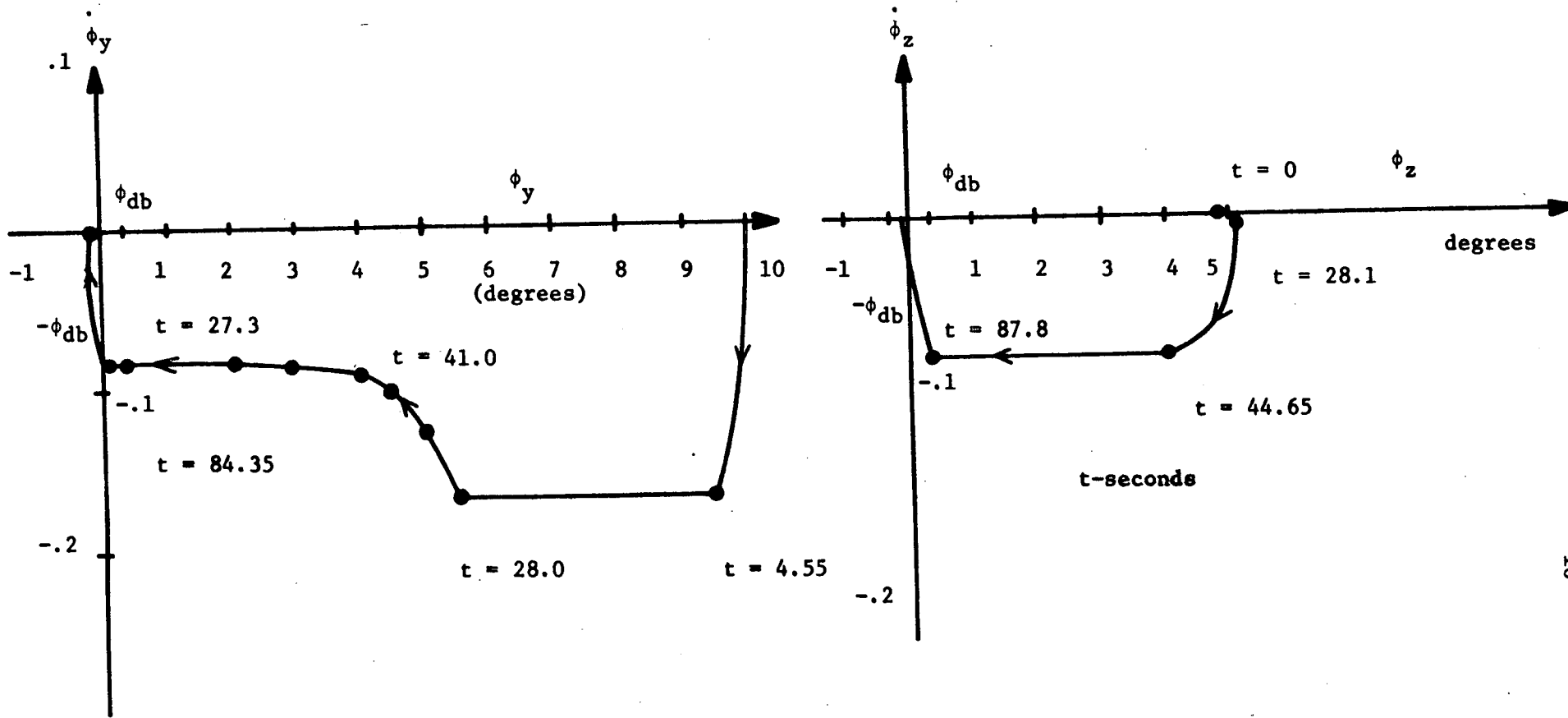


Figure II-7. Boundaries of No-Fire Region for RCJ System Using Sum and Difference Saturation Signals.



INITIAL CONDITIONS

$\phi_{y0} = 10.0^\circ$   
 $\dot{\phi}_{y0} = 0.0^\circ/\text{sec}$   
 $\phi_{z0} = 5.0^\circ$   
 $\dot{\phi}_{z0} = 0.0^\circ/\text{sec}$

DESIGN PARAMETERS

$\phi_{db} = \pm 0.3^\circ$   
 $M_y = .0391$   
 $M_z = .0378$   
 $A_{1y} = 4.080$   
 $A_{1z} = 4.176$   
 RATE LEDGE = 0.172

RESULTS

1. Time to reach and remain inside deadband:  
 y - 84.35 sec  
 z - 87.8 sec
2. Fuel consumption at:  
 84.35 sec: 27.3  
 87.8 sec: 27.3  
 (1 unit is the energy consumed by one thruster firing for one sec)

Figure II-8. Phase-Plane Trajectories of RCJ System--Sum and Difference Saturation Signal

Comparing the data presented in Figures II-4 and II-8, it can be seen that the modified system is slower but the fuel consumption (based on both the  $\phi_y$  and  $\phi_z$  errors being less than the deadband value) is reduced. Further work is needed to determine if the rate-ledge and feedback gains can be changed so that the modified system has comparable speed of response with less fuel consumption. It should be noted that with this modification the  $(\phi_z + \phi_y)$  controller and the  $(\phi_y - \phi_z)$  controller are decoupled even when the saturation limits are active; thrusters 11, 12, 15, 16 are active for  $(\phi_z + \phi_y)$  errors and thrusters 9, 10, 13, 14 are active for  $(\phi_z - \phi_y)$  errors.

### III. THE CONTROL MOMENT GYRO ATTITUDE CONTROL SYSTEM

The control moment gyro (CMG) attitude control system also controls the angles  $\phi_x$ ,  $\phi_y$ ,  $\phi_z$ . The control system simulated in this study uses the optimal steering law proposed in [4]. The CMG cluster arrangement is shown in Figure III-1. Part A of this section gives the block diagram and system equations in matrix form as taken from [4]. Part B is a general state-variable analysis to determine the general structure of the input and feedback matrices that will decouple the X, Y, and Z axes.

#### Part A. System Simulation Using the Optimal Steering Law [4]

A block diagram of the system is shown in Figure III-2. With the outer gimbals clamped, the outer gimbal rates  $\dot{\delta}_3(1)$ ,  $\dot{\delta}_3(2)$ ,  $\dot{\delta}_3(3)$  are zero. The equations for the reaction moments, in matrix form, are:

$$\begin{bmatrix} M_{RXV} \\ M_{RYV} \\ M_{RZV} \end{bmatrix} = [A] \begin{bmatrix} \dot{\delta}_1(1) \\ \dot{\delta}_1(2) \\ \dot{\delta}_1(3) \end{bmatrix}, \text{ where} \quad (\text{III-1})$$

$$[A] = \begin{bmatrix} \sin(\delta_1(1))\cos(\delta_3(1)) & \cos(\delta_1(2)) & -\sin(\delta_1(3))\sin(\delta_3(3)) \\ -\sin(\delta_1(1))\sin(\delta_3(1)) & \sin(\delta_1(2))\cos(\delta_3(2)) & \cos(\delta_1(3)) \\ \cos(\delta_1(1)) & -\sin(\delta_1(2))\sin(\delta_3(2)) & \sin(\delta_1(3))\cos(\delta_3(3)) \end{bmatrix} \quad (\text{III-2})$$

The steering law  $[T_S]$  gives the commanded gimbal rates in terms of the commanded moments.

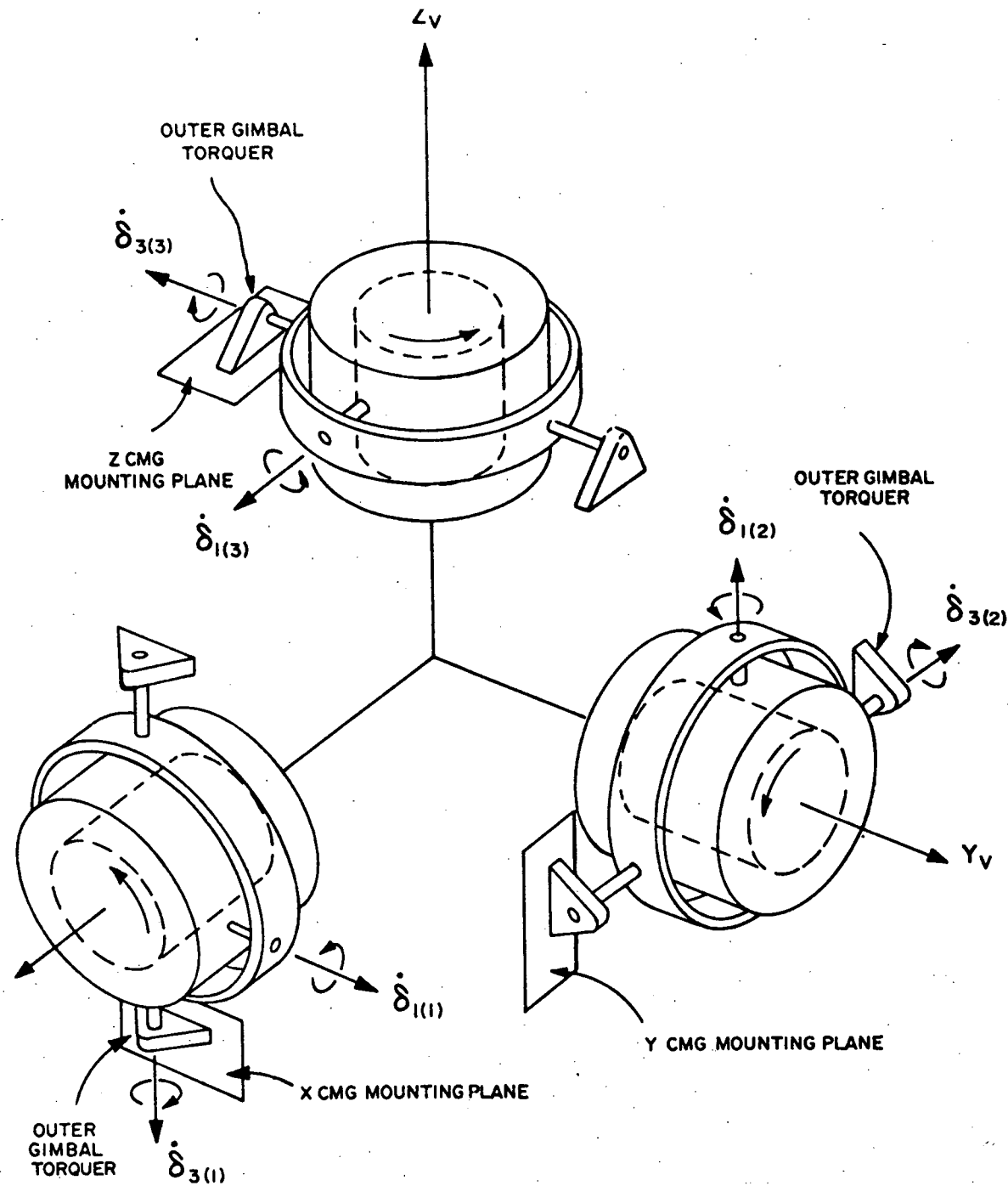


Figure III-1. CMG Cluster.

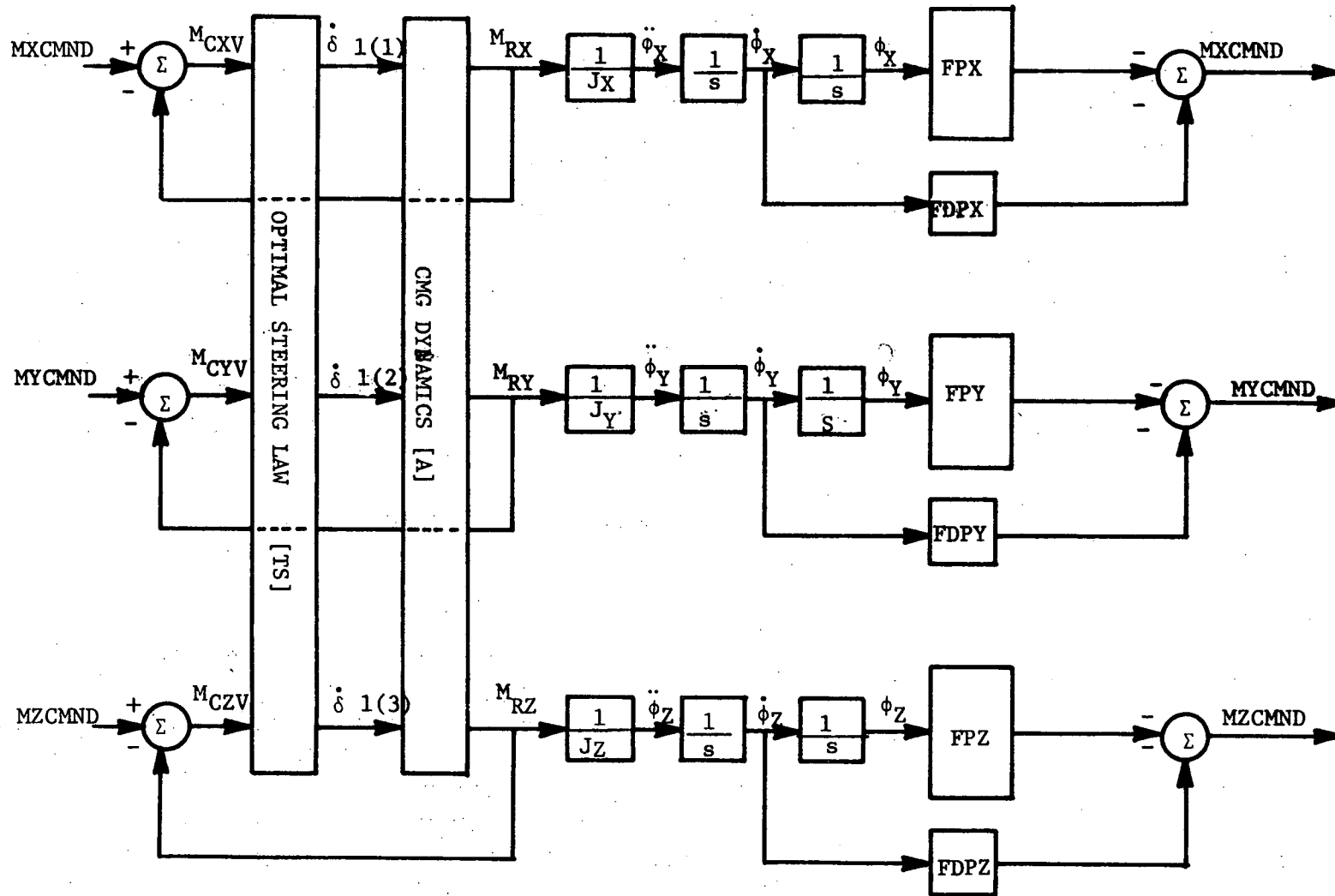


Figure III - 2 CMG System Block Diagram

$$\begin{bmatrix} \dot{\delta}1(1)_c \\ \dot{\delta}1(2)_c \\ \dot{\delta}1(3)_c \end{bmatrix} = [T_S] \begin{bmatrix} M_{CXV} \\ M_{CYV} \\ M_{CZV} \end{bmatrix} \quad (\text{III-3})$$

Assuming that the actual gimbal rates are equal to the commanded gimbal rates, the relationship between the commanded moment and the reaction moment is:

$$\begin{bmatrix} M_{RXV} \\ M_{RYV} \\ M_{RZV} \end{bmatrix} = [A] [T_S] \begin{bmatrix} M_{CXV} \\ M_{CYV} \\ M_{CZV} \end{bmatrix} \quad (\text{III-4})$$

It is desirable that the reaction moment equal the commanded moment, which requires that:

$$[A][T_S] = [I], \text{ where } [I] \text{ is the identity matrix.} \quad (\text{III-5})$$

The steering law is thus given by

$[T_S] = [A]^{-1}$ , where  $[A]^{-1}$  is the inverse of the matrix A. It should be noted that [A] is singular at some operating conditions.

There is one vehicle control loop for each of the three axes. A rate-plus-position feedback is used for each of the vehicle control

loops. The vehicle control law output is processed to obtain the moment command. This moment command is compared to the actual moment and the error is used together with the optimal steering law, to provide the proper reaction moment on the vehicle.

A digital computer simulation of the three axis CMG attitude control system has been written and is included in the Appendix.

#### Part B. A State-Space Analysis of the CMG System (Clamped Mode) for Axis Decoupling

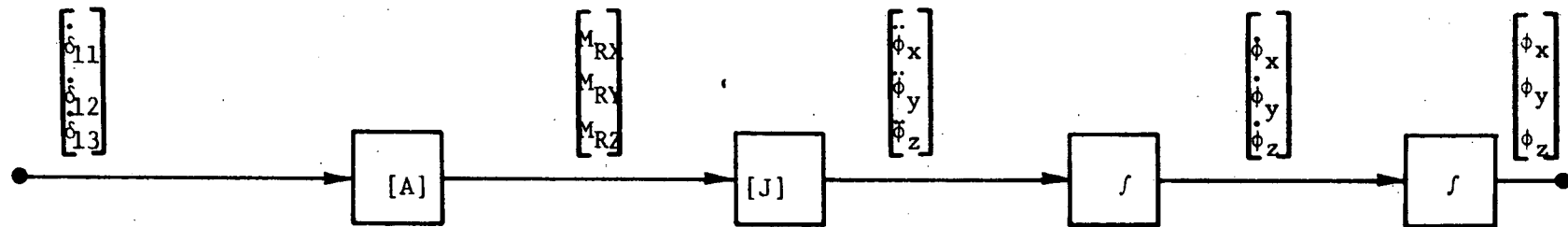
The object of this analysis is to write the system equations in state-space form and determine the form of the input matrices and the feedback matrices that will minimize or eliminate the coupling between the X, Y, and Z axes. In the first phase of the study the torque motor dynamics are neglected but are included in the second phase.

##### Phase 1. Torque Motor Dynamics Neglected

The open-loop system is shown in Figure III-3. Let the states and the inputs be defined as

$$\underline{x} = \begin{bmatrix} x_1 \\ x_2 \\ x_3 \\ x_4 \\ x_5 \\ x_6 \end{bmatrix} = \begin{bmatrix} \phi_x \\ \dot{\phi}_x \\ \phi_y \\ \dot{\phi}_y \\ \phi_z \\ \dot{\phi}_z \end{bmatrix} ; \text{ the input, } \underline{u} = \begin{bmatrix} u_1 \\ u_2 \\ u_3 \end{bmatrix} = \begin{bmatrix} \dot{\delta}_{11} \\ \dot{\delta}_{12} \\ \dot{\delta}_{13} \end{bmatrix} \quad (\text{III-6})$$





where

$$[A] = \begin{bmatrix} \cos \delta_{31} \sin \delta_{11} & \cos \delta_{12} & -\sin \delta_{33} \sin \delta_{13} \\ -\sin \delta_{31} \sin \delta_{11} & \cos \delta_{32} \sin \delta_{12} & \cos \delta_{13} \\ \cos \delta_{11} & -\sin \delta_{32} \sin \delta_{12} & \cos \delta_{33} \sin \delta_{13} \end{bmatrix}$$

$$[J] = \begin{bmatrix} \frac{1}{J_x} & 0 & 0 \\ 0 & 1/J_y & 0 \\ 0 & 0 & 1/J_z \end{bmatrix}$$

Fig. III - 3. Block Diagram of Open-loop CMG System; Clamped Mode and Torque Motor Dynamics Neglected

Then the state-space equation is

$$\dot{\underline{x}} = [A_0] \underline{x} + [B] \underline{u} \quad (\text{III-7})$$

where

$$[A_0] = \begin{bmatrix} 0 & 1 & 0 & 0 & 0 & 0 \\ 0 & 0 & 0 & 0 & 0 & 0 \\ 0 & 0 & 0 & 1 & 0 & 0 \\ 0 & 0 & 0 & 0 & 0 & 0 \\ 0 & 0 & 0 & 0 & 0 & 1 \\ 0 & 0 & 0 & 0 & 0 & 0 \end{bmatrix} \quad (\text{III-8})$$

$$[B] = \begin{bmatrix} 0 & 0 & 0 \\ 1 & 0 & 0 \\ 0 & 0 & 0 \\ 0 & 1 & 0 \\ 0 & 0 & 0 \\ 0 & 0 & 1 \end{bmatrix} \quad [J][A] \quad (\text{III-9})$$

$\begin{matrix} 6 \times 3 & & 3 \times 3 & 3 \times 3 \\ & & & 6 \times 3 \end{matrix}$

To decouple the axes let

$$\underline{u} = [T_s] \underline{\phi}_c + [F_1] \underline{x} \quad \text{where} \quad \underline{\phi}_c = \begin{bmatrix} \phi_{cx} \\ \phi_{cy} \\ \phi_{cz} \end{bmatrix} = \text{desired output angles and} \quad (\text{III-10})$$

$\begin{matrix} 3 \times 3 & & 3 \times 6 \end{matrix}$

$[T_s]$  and  $[F_1]$  are decoupling matrices.

Then

$$\dot{\underline{x}} = \{[A^0] + [B][F_1]\} \underline{x} + [B] [Ts] \underline{\phi}^c \quad (\text{III-11})$$

For the axes to be decoupled,  $[B][Ts]$  must have the form

$$\begin{bmatrix} 0 & 0 & 0 \\ \gamma_{21} & 0 & 0 \\ 0 & 0 & 0 \\ 0 & \gamma_{42} & 0 \\ 0 & 0 & 0 \\ 0 & 0 & \gamma_{63} \end{bmatrix}$$

where the  $\gamma$ 's are nonzero.

$$\text{Thus } [B][Ts] = \begin{bmatrix} 0 & 0 & 0 \\ \gamma_{21} & 0 & 0 \\ 0 & 0 & 0 \\ 0 & \gamma_{42} & 0 \\ 0 & 0 & 0 \\ 0 & 0 & \gamma_{63} \end{bmatrix} = \begin{bmatrix} 0 & 0 & 0 \\ 1 & 0 & 0 \\ 0 & 0 & 0 \\ 0 & 1 & 0 \\ 0 & 0 & 0 \\ 0 & 0 & 1 \end{bmatrix} [J][A][Ts] \quad (\text{III-12})$$

[J] is a diagonal matrix of full rank, so this condition can be satisfied only if [A][Ts] is a diagonal matrix of full rank.

In addition, [A<sub>o</sub>] + [B][F<sub>1</sub>] must have the form

$$\begin{bmatrix} \alpha_{11} & \alpha_{12} & 0 & 0 & 0 & 0 \\ \alpha_{21} & \alpha_{22} & 0 & 0 & 0 & 0 \\ 0 & 0 & \alpha_{33} & \alpha_{34} & 0 & 0 \\ 0 & 0 & \alpha_{43} & \alpha_{44} & 0 & 0 \\ 0 & 0 & 0 & 0 & \alpha_{55} & \alpha_{56} \\ 0 & 0 & 0 & 0 & \alpha_{65} & \alpha_{66} \end{bmatrix}$$

where same  $\alpha$ 's in each sub-block are nonzero. Since [A<sub>o</sub>] has the above form, then [B][F<sub>1</sub>] must also have the above form.

$$\text{Thus } [B][F_1] = \begin{bmatrix} \alpha_{11} & \alpha_{12} & 0 & 0 & 0 & 0 \\ \alpha_{21} & \alpha_{22} & 0 & 0 & 0 & 0 \\ 0 & 0 & \alpha_{33} & \alpha_{34} & 0 & 0 \\ 0 & 0 & \alpha_{43} & \alpha_{44} & 0 & 0 \\ 0 & 0 & 0 & 0 & \alpha_{55} & \alpha_{56} \\ 0 & 0 & 0 & 0 & \alpha_{65} & \alpha_{66} \end{bmatrix} = \quad (\text{III-13})$$

$$\begin{bmatrix} 0 & 0 & 0 \\ 1 & 0 & 0 \\ 0 & 0 & 0 \\ 0 & 1 & 0 \\ 0 & 0 & 0 \\ 0 & 0 & 1 \end{bmatrix} \quad [J][A][F_1] \quad (\text{III-14})$$

This implies that  $[A][F_1]$  must have the form

$$\begin{bmatrix} B_{11} & B_{12} & 0 & 0 & 0 & 0 \\ 0 & 0 & B_{23} & B_{24} & 0 & 0 \\ 0 & 0 & 0 & 0 & B_{35} & B_{36} \end{bmatrix}$$

where a B in each row must be nonzero to have a feedback signal.

Thus the conditions for axes decoupling are that

- (1)  $[A][T_s]$  be a diagonal matrix
- (2)  $[A][F_1]$  have the form

$$\begin{bmatrix} B_{11} & B_{12} & 0 & 0 & 0 & 0 \\ 0 & 0 & B_{23} & B_{24} & 0 & 0 \\ 0 & 0 & 0 & 0 & B_{35} & B_{36} \end{bmatrix}$$

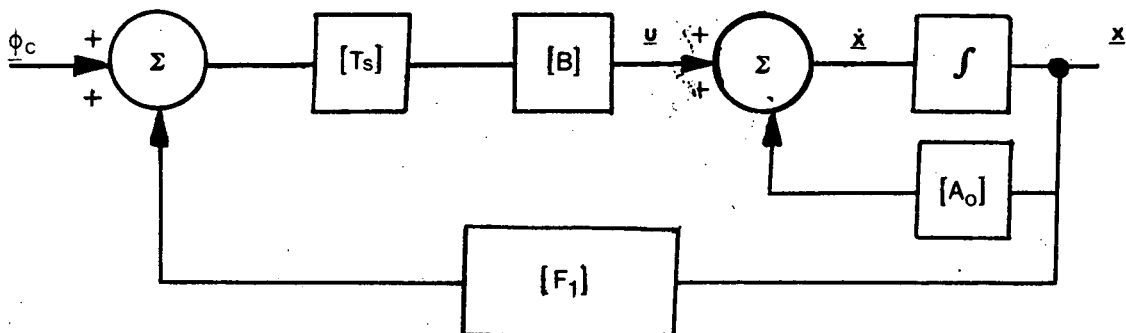
Note that if

$$B_{12} = \text{a constant times } B_{11}$$

$$B_{24} = \text{" " " " } B_{23}$$

$$B_{36} = \text{" " " " } B_{35}$$

then the feedback is proportional-plus-rate and the decoupling can be achieved as shown.



$$\text{where } [F_1] = \begin{bmatrix} 1 & A_{1x} & 0 & 0 & 0 & 0 \\ 0 & 0 & 1 & A_{1y} & 0 & 0 \\ 0 & 0 & 0 & 0 & 1 & A_{1z} \end{bmatrix}$$

If  $[A][Ts] = [I]$ , the identity matrix, then this implements the optimal control law of [4].

### Phase 2. Torque Motor Dynamics Included

Assuming that the torque motors can be represented as first-order systems with time-constants,  $T_m$ , the open-loop diagram is as shown in Figure III-4 where  $u_1, u_2, u_3$  are the input signals to the torque motors.

The states and the input vectors are

$$\begin{bmatrix} \underline{x} \\ \underline{z} \end{bmatrix} = \begin{bmatrix} \phi_x \\ \dot{\phi}_x \\ \phi_y \\ \dot{\phi}_y \\ \phi_z \\ \dot{\phi}_z \\ \dot{\delta}_{11} \\ \dot{\delta}_{12} \\ \dot{\delta}_{13} \end{bmatrix}; \quad \underline{u} = \begin{bmatrix} u_1 \\ u_2 \\ u_3 \end{bmatrix} = \text{input to the torque motors} \quad (\text{III-15})$$

Then the state-space equation is

$$\begin{bmatrix} \dot{\underline{x}} \\ \dot{\underline{z}} \end{bmatrix} = \begin{bmatrix} [A_o] & [B] \\ [0] & -\frac{1}{T_m} [I] \end{bmatrix} \begin{bmatrix} \underline{x} \\ \underline{z} \end{bmatrix} + \begin{bmatrix} [0] \\ \frac{1}{T_m} [I] \end{bmatrix} \underline{u} \quad (\text{III-16})$$

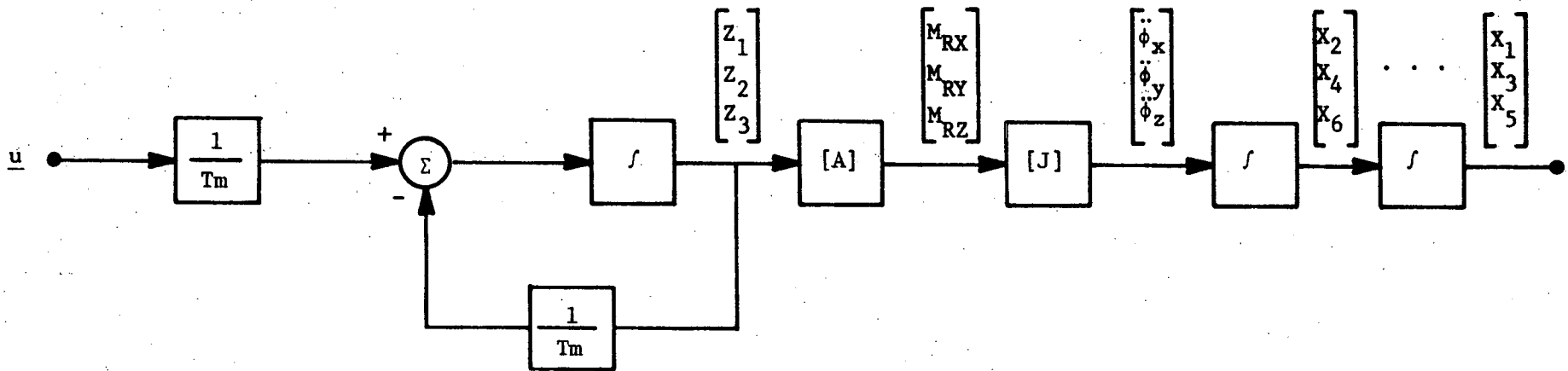


Figure III-4. Block Diagram of Open-loop CMG System; Clamped Mode and Torque Motor Dynamics Included

To decouple the axes let

$$\underline{u} = [Ts] \underline{\phi}c + \begin{bmatrix} [F_1] \\ [F_2] \end{bmatrix} \begin{bmatrix} \underline{x} \\ \underline{z} \end{bmatrix} \quad (\text{III-17})$$

$$= [Ts] \underline{\phi}c + [F_1] \underline{x} + [F_2] \underline{z} \quad (\text{III-18})$$

Thus

$$\dot{\underline{x}} = [A_0] \underline{x} + [B] \underline{z} \quad (\text{III-19})$$

$$\underline{z} = \frac{1}{T_m} [F_2 - I] \underline{z} + \frac{1}{T_m} [F_1] \underline{x} + \frac{1}{T_m} [Ts] \underline{\phi}c \quad (\text{III-20})$$

Assume that  $[A]$ ,  $[Ts]$ ,  $[F_1]$ , and  $[F_2]$  are constant matrices for small changes about a steady-state operating point. Then

$$\ddot{\underline{x}} = [A_0] \dot{\underline{x}} + [B] \dot{\underline{z}} \quad (\text{III-21})$$

$$= \left\{ [A_0]^2 + \frac{1}{T_m} [B] [F_1] \right\} \underline{x} + \left\{ [A_0] [B] + \frac{1}{T_m} [B] [F_2 - I] \right\} \underline{z} + \frac{1}{T_m} [B] [Ts] \underline{\phi}c \quad (\text{III-22})$$

To decouple the axes,  $[B][Ts]$  must have the same form as in Part A and as before  $[A][Ts]$  must be a diagonal matrix.

Continuing,

$$\begin{aligned} \ddot{\underline{x}} = & \left\{ [A_0]^3 + \frac{1}{T_m} [B] [F_1] [A_0] + \frac{1}{T_m} [A] [B] [F_1] + \frac{1}{T_m^2} [B] [F_2 - I] [F_1] \right\} \underline{x} + \\ & \left\{ [A_0]^2 [B] + \frac{1}{T_m} [B] [F_1] [B] + \frac{1}{T_m} [A] [B] [F_2 - I] + \frac{1}{T_m^2} [B] [F_2 - I]^2 \right\} \underline{z} + \\ & \left\{ \frac{1}{T_m} [A_0] [B] [Ts] + \frac{1}{T_m^2} [B] [F_2 - I] [Ts] \right\} \underline{\phi}c + \frac{1}{T_m} [B] [Ts] \dot{\underline{\phi}}c \quad (\text{III-23}) \end{aligned}$$



To decouple the axes,  $\frac{1}{T_m}[A_0][B][Ts] + \frac{1}{T_m^2}[B][F_2 - I][Ts]$  must have the form

$$\begin{array}{ccc|c} \gamma_{11} & 0 & 0 & \\ \gamma_{21} & 0 & 0 & \\ 0 & \gamma_{32} & 0 & \\ 0 & \gamma_{42} & 0 & \\ 0 & 0 & \gamma_{53} & \\ 0 & 0 & \gamma_{63} & \end{array} \quad ; \text{ a } \gamma_{ij} \text{ in each sub-block is nonzero}$$

The previous condition stipulates that  $[B][Ts]$  have this form. It is easy to show that  $[A_0][B][Ts]$  has this form. Therefore  $[B][F_2][Ts]$  must also have this form. This condition is satisfied if  $[F_2]$  is equal to a constant times the identity matrix.

$$\text{Let } [F_2 - I] = k_2[I] \quad (\text{III-24})$$

then

$$\dot{\underline{z}} = \frac{k_2}{T_m} \underline{z} + \frac{1}{T_m} [F_1] \underline{x} + \frac{[Ts]}{T_m} \phi_c \quad (\text{III-25})$$

and

$$[B]\dot{\underline{z}} = \frac{k_2}{T_m} [B]\underline{z} + \frac{[B][F_1]}{T_m} \underline{x} + \frac{[B][Ts]}{T_m} \phi_c \quad (\text{III-26})$$

and solving (III-19) for  $[B]\underline{z}$  gives

$$[B]\dot{\underline{z}} = \frac{k_2}{T_m} \dot{\underline{x}} + \left( \frac{[B][F_1]}{T_m} - \frac{k_2}{T_m} [A_0] \right) \underline{x} + \frac{[B][Ts]}{T_m} \phi_c \quad (\text{III-27})$$

This substituted into (III-21) yields

$$\ddot{\underline{X}} = \{[A_0] + \frac{k_2[I]}{T_m}\} \dot{\underline{X}} + \{\frac{[B][F_1]}{T_m} - \frac{k_2}{T_m} [A_0]\} \underline{X} + \frac{[B][T_s]}{T_m} \phi_c \quad (\text{III-28})$$

This equation yields an additional requirement for decoupling;  $[B][F_1]$  must have the form

$$\begin{bmatrix} \alpha_{11} & \alpha_{12} & 0 & 0 & 0 & 0 \\ \alpha_{21} & \alpha_{22} & 0 & 0 & 0 & 0 \\ 0 & 0 & \alpha_{33} & \alpha_{34} & 0 & 0 \\ 0 & 0 & \alpha_{43} & \alpha_{44} & 0 & 0 \\ 0 & 0 & 0 & 0 & \alpha_{55} & \alpha_{56} \\ 0 & 0 & 0 & 0 & \alpha_{65} & \alpha_{66} \end{bmatrix}$$

where some  $\alpha$ 's in each block are nonzero.

This result is the same as that derived in Part A and implies that

$[A][F_1]$  must have the form

$$\begin{bmatrix} B_{11} & B_{12} & 0 & 0 & 0 & 0 \\ 0 & 0 & B_{23} & B_{24} & 0 & 0 \\ 0 & 0 & 0 & 0 & B_{35} & B_{36} \end{bmatrix}$$

as was the case in Part A

To summarize, the necessary structure of the matrices to decouple the axes is that

- (1)  $[A][Ts]$  must be a diagonal matrix
- (2)  $[F_2]$  must be a constant times the identity matrix
- (3)  $[A][F_1]$  must have the form

$$\begin{bmatrix} B_{11} & B_{12} & 0 & 0 & 0 & 0 \\ 0 & 0 & B_{23} & B_{24} & 0 & 0 \\ 0 & 0 & 0 & 0 & B_{35} & B_{36} \end{bmatrix}$$

The system with feedback is shown in Figure III-5.

With proportional-plus-rate feedback the system takes the form of Figure III-6. In this form the  $[F_2]$  matrix, a  $k_2[I]$  matrix, does not aid in the axes decoupling. However, if this diagram is redrawn in terms of the original set of variables in a modified form, Figure III-7, where it is assumed  $[Ts]$  is non-singular, then since it is desirable that  $[Ts][A] \approx [I]$   $[Ts]^{-1} = [A]$ , the system can be implemented as shown in Figure III-8. This is the system implemented in [4] with the objective that  $[Ts][A] = [I]$ . However, this cannot be accomplished under all conditions since  $[A]$  is singular (and thus  $[Ts]$ ) at some operating conditions. This problem is minimized in [4] by proper selection of the angles at which the outer gimbals are clamped and by placing a limit on the minimum value of  $|\det [A]|$  used in the computation of  $[Ts]$ .

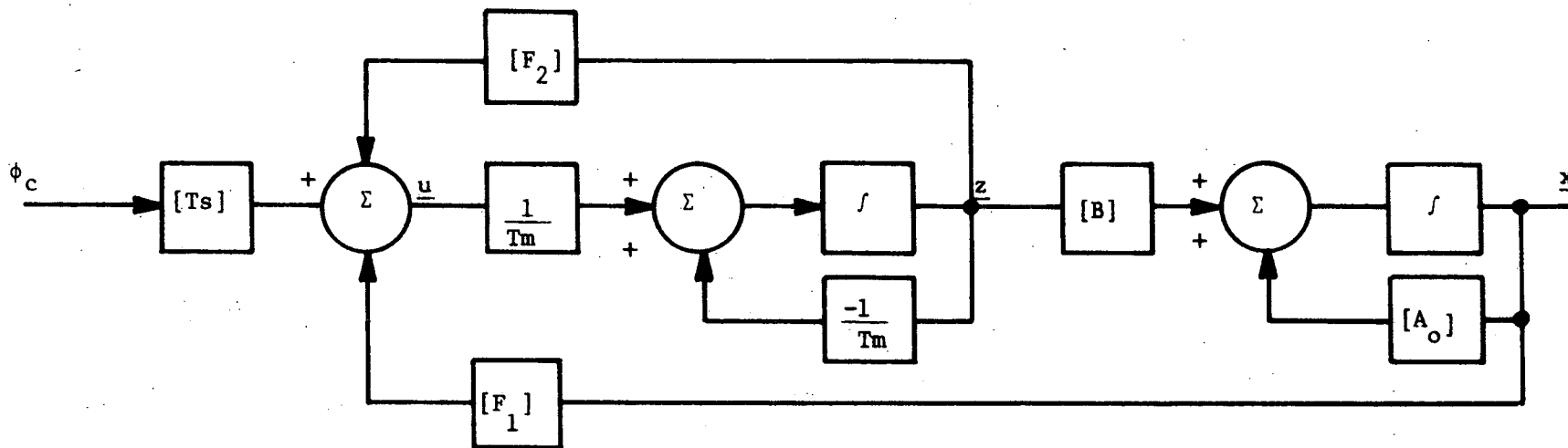


Figure III-5. CMG Closed-loop System; Clamped Mode

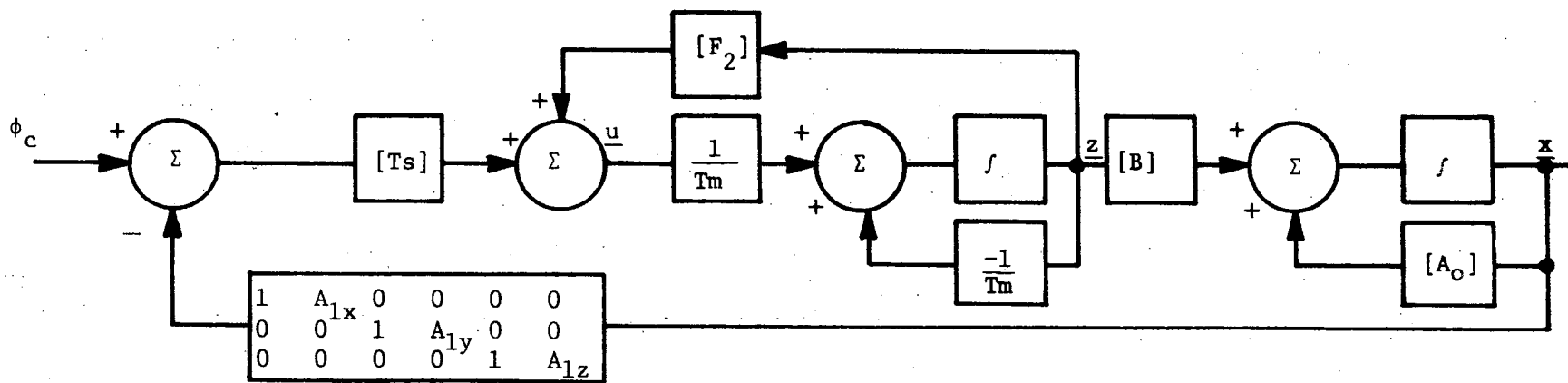


Figure III-6. CMG Closed-loop System with Proportional-plus-Rate Feedback; Clamped Mode.

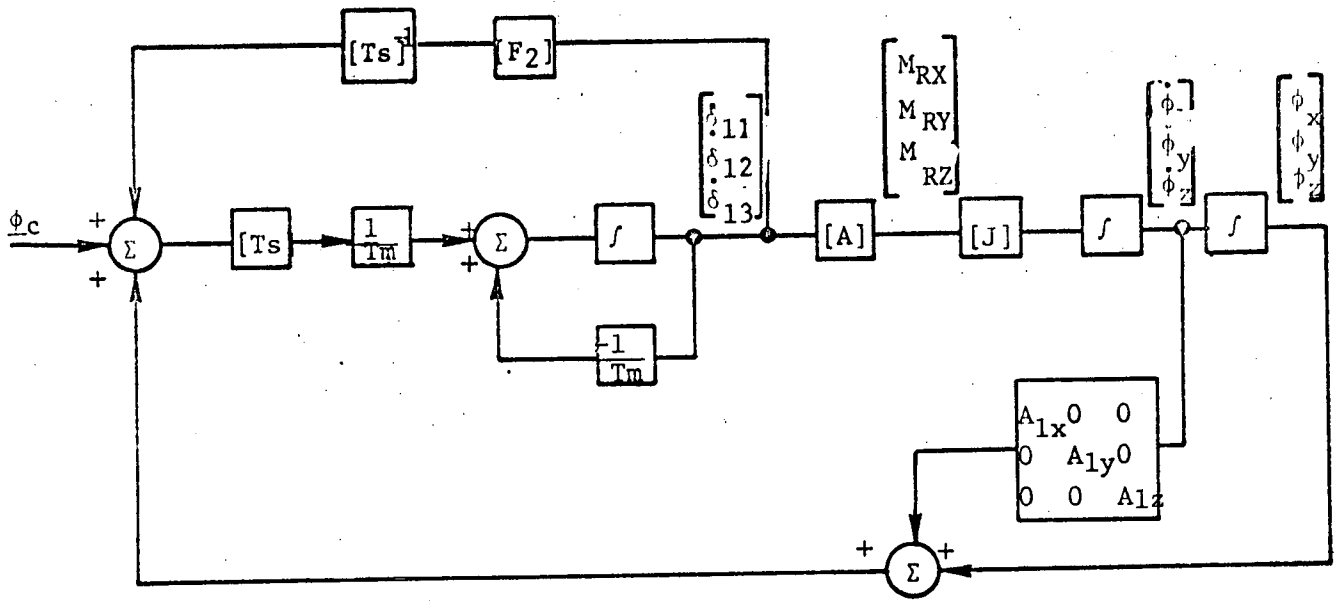


Figure III-7. Closed-loop System; Proportional-plus-rate Feedback; Clamped Mode

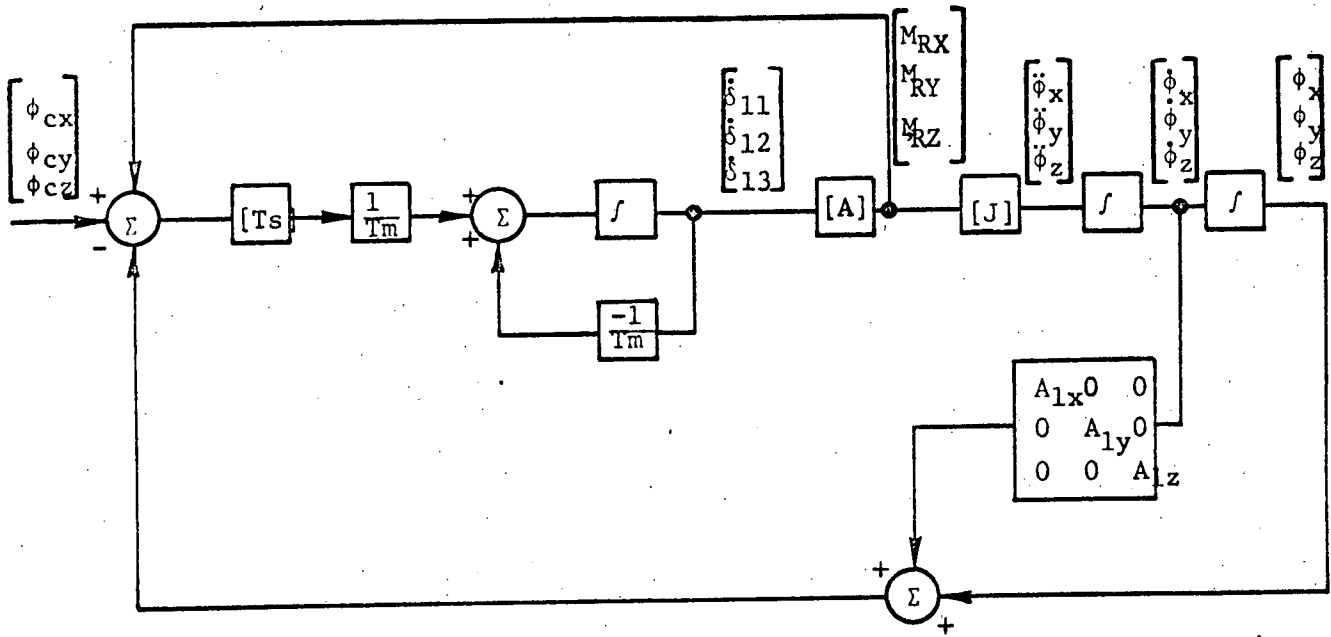


Figure III-8. Closed-loop System; Proportional-plus-rate Feedback; Clamped Mode

#### IV. COMBINED REACTION CONTROL JET AND CONTROL MOMENT GYRO ATTITUDE CONTROL SYSTEM

The reaction control jet (RCJ) attitude control system and the control moment gyro (CMG) attitude control system are combined to operate as a single attitude control system. The objective was to mate the systems so that the torques generated by each system are never in opposition, speed of response is improved, and fuel consumption by the RCJ system is reduced.

The RCJ system uses the sum and difference feedback control described in Section II of this report. The CMG system uses the same sum and difference feedback signals as are generated in the RCJ system,  $\epsilon_x$ ,  $\epsilon_y$ ,  $\epsilon_z$ . A block diagram of the CMG system is shown in Figure IV-1. The saturation blocks in the position feedback paths are used to place the CMG torque reversal lines in the center of the RCJ no-fire regions. The phase-plane plot of the no-fire boundaries of the X-axis and a typical response are shown in Figure IV-2. A phase-plane plot of the no-fire region of the sum ( $\phi_z + \phi_y$ ) and the difference ( $\phi_z - \phi_y$ ) systems and a typical response are shown in Figure IV-3. The same data plotted for each axis is shown in Figure IV-4.

The CMG system torques aid the RCJ system torques whenever the RCJ's are firing and the CMG torques tend to hold the RCJ system inside the no-fire regions. A digital computer program to simulate the combined systems is described in the Appendix.

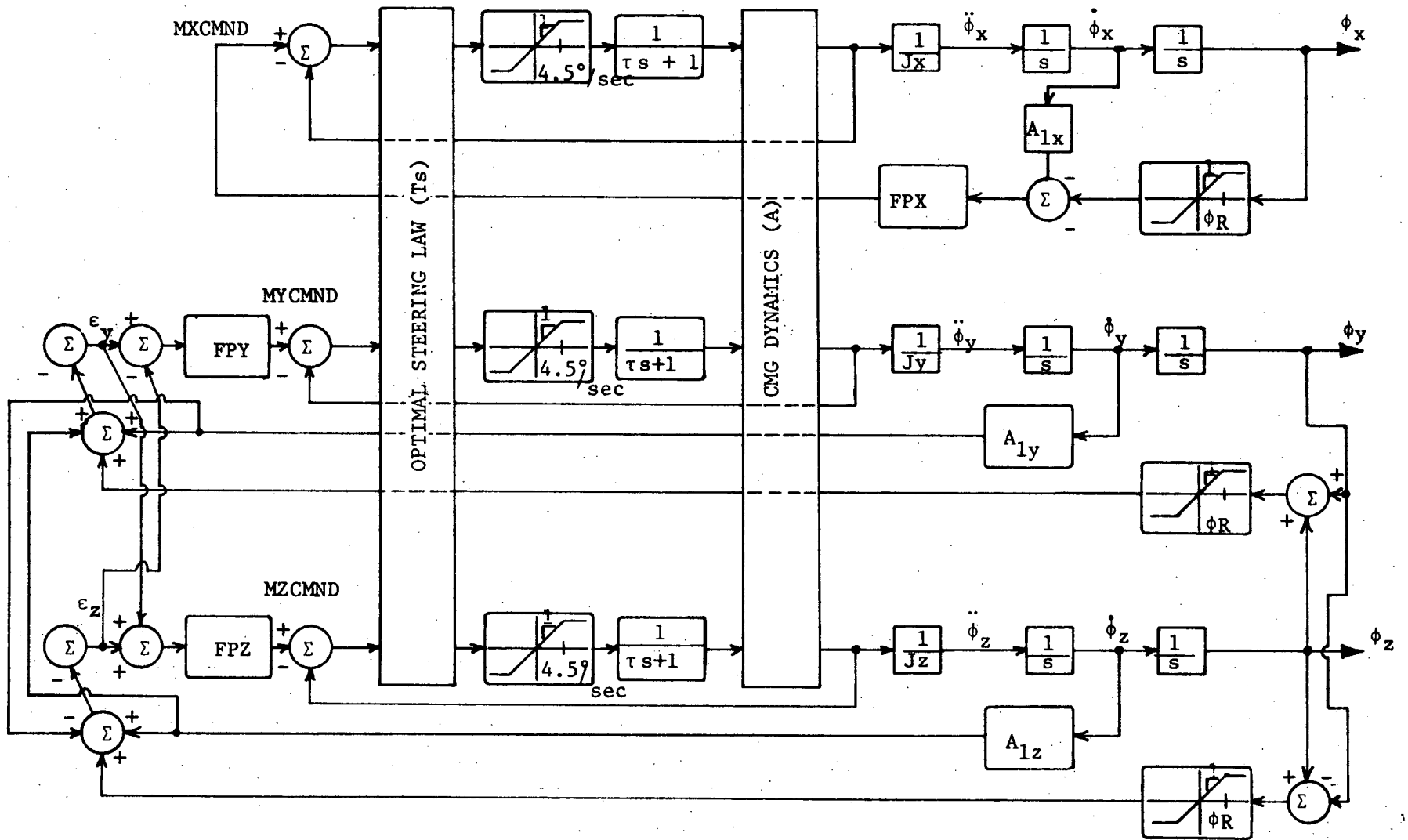


Figure IV-1. CMG System with Sum and Difference Saturation Signals.

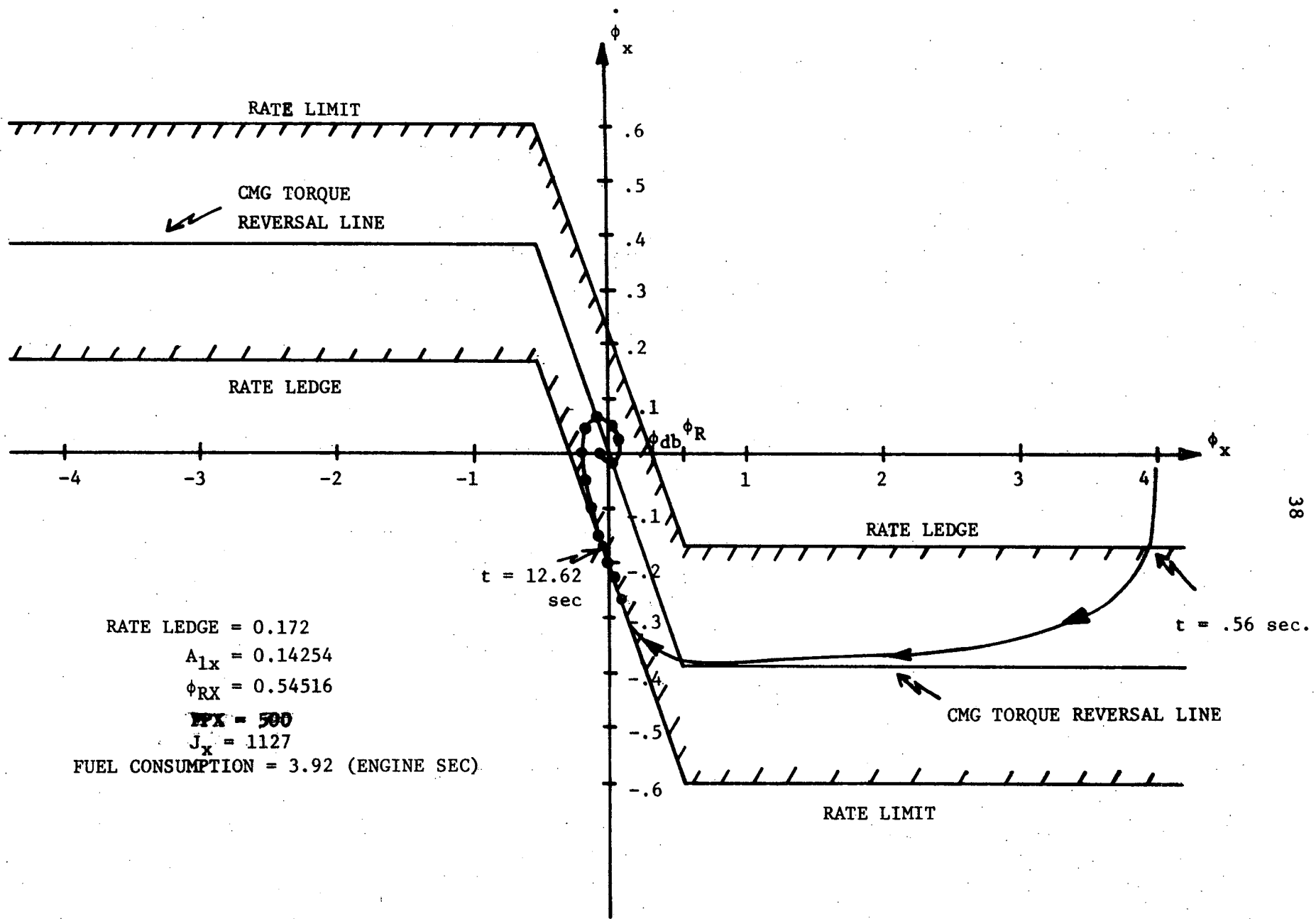
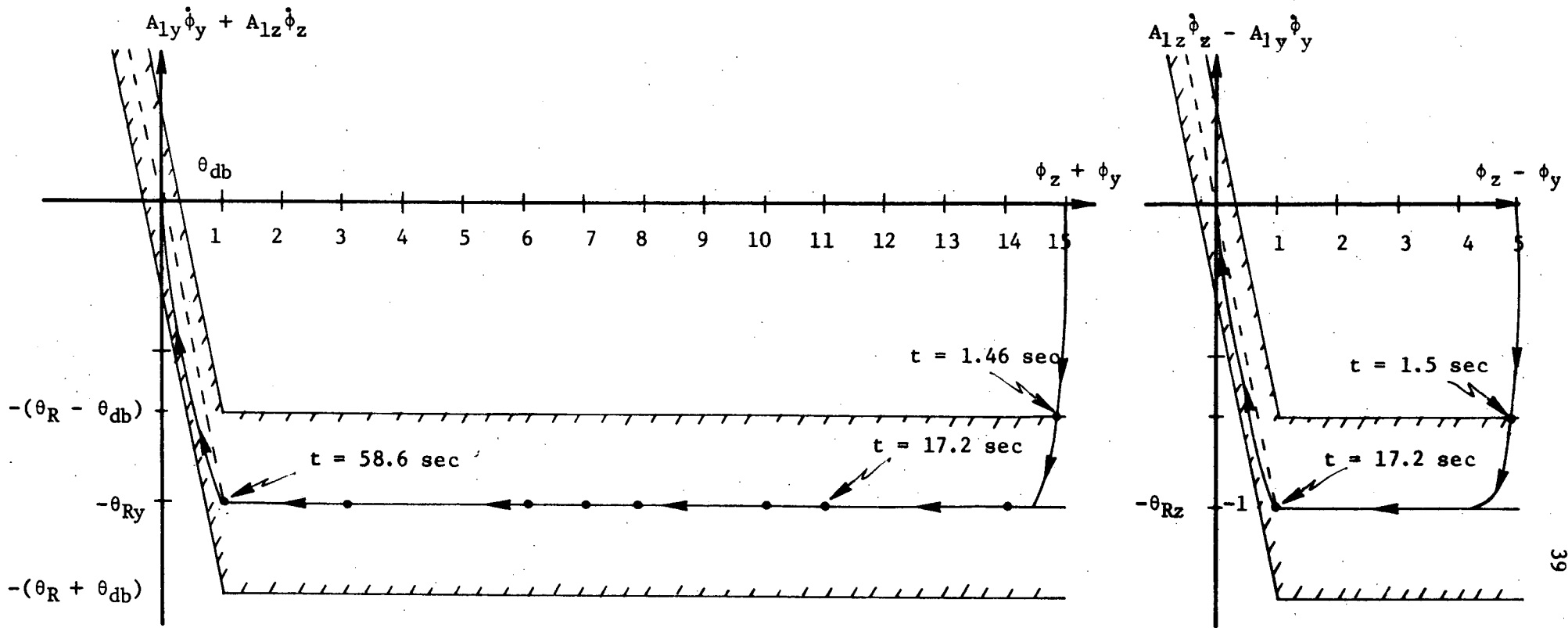


Figure IV-2. Phase-Plane Trajectory of Combined RCJ and CMG System





INITIAL CONDITIONS

$\phi_{y0} = 10^\circ$   
 $\phi_{y0} = 0$   
 $\phi_{z0} = 5^\circ$   
 $\phi_{z0} = 0$

DESIGN PARAMETERS

$\phi_{db} = \pm 3^\circ$   
 RATE LEDGE = .172  
 $M_y = .0391$   
 $M_z = .0378$   
 $A_{1y} = 4.080$   
 $A_{1z} = 4.1757$   
 $\phi_{Ry} = 1.0018$   
 $\phi_{Rz} = 1.0182$   
 $FPY = 1000$   
 $FPZ = 1000$   
 $J_y = 2947$   
 $J_z = 2918$

RESULTS

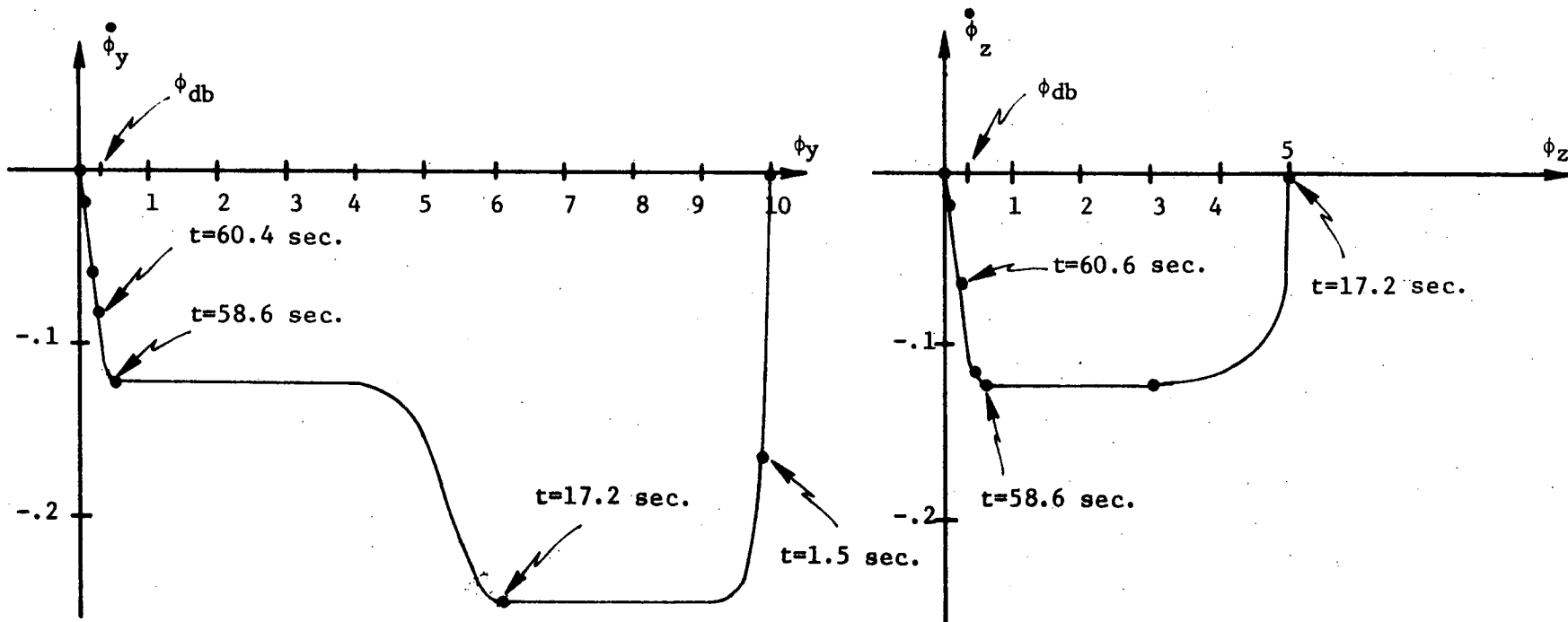
1. Time to reach and remain inside deadband

$\phi_x + \phi_y$  - 63.0 sec  
 $\phi_x - \phi_y$  - 21.4 sec

2. Fuel consumption at

63.0 sec - 5.92 Engine-sec  
 21.4 sec - 5.92 Engine-sec

Figure IV-3. Phase-Plane Trajectories of Combined RCJ and CMG Systems



INITIAL CONDITIONS

$\phi_{y0} = 10^\circ$   
 $\dot{\phi}_{y0} = 0^\circ/\text{sec.}$   
 $\phi_{z0} = 5^\circ$   
 $\dot{\phi}_{z0} = 0^\circ/\text{sec.}$

DESIGN PARAMETERS

$\phi_{db} = \pm .3^\circ$   
 RATE LEDGE = .172  
 $M_y = .0391$   
 $M_z = .0378$   
 $A_{1y} = 4.080$   
 $A_{1z} = 4.1757$   
 $\phi_{RY} = 1.0018$   
 $\phi_{RZ} = 1.0182$   
 $FPY = 1000$   
 $FPZ = 1000$   
 $J_y = 2947$   
 $J_z = 2918$

RESULTS

1. Time to reach and remain inside deadband:  
 Y - 60.4 sec.  
 Z - 60.6 sec.
2. Fuel consumption at  
 60.4 - 5.92  
 60.6 - 5.92  
 (One unit is the energy consumed by one thruster firing for one second.)

Figure IV-4. Phase-Plane Trajectories of Combined RCJ and CMG Systems

## V. COMPUTATION OF DISTURBING TORQUES DUE TO MOTION OF THE TELEVISION CAMERA

The proposed CARD spacecraft has an on-board television camera which is used during orbiting or landing to view the terrain and proposed landing sites. The TV camera and its mount are constructed to permit rotation about two axes. The purpose of this section is to develop a procedure for computing the torques about the spacecraft center-of-mass produced by motion of the television camera.

The general shape, dimensions, and mass of the TV camera and its mount are scaled from Figure 4.5 and Figure 4.83 of Reference 1. Based on these figures the TV camera and mount are assumed to have the general form and dimensions of Figure V-1. It will be treated as a rigid, homogeneous mass. The XY plane is a plane of symmetry and the XYZ coordinates of Figure V-1 are parallel to the spacecraft XYZ coordinates.

The additional assumptions made are:

1. The spacecraft (main portion) angular velocities are small compared to the relative angular velocities of the television camera.
2. The motion of the system (main portion plus the TV camera) center-of-mass due to TV camera rotation may be neglected in computing inertia characteristics.

### Part A. Derivation of Torque Equations\*

The inertia matrix of the TV camera and mount is

\*This approach was outlined by Dr. John E. Cochran, Assistant Professor of Aerospace Engineering, Auburn University.

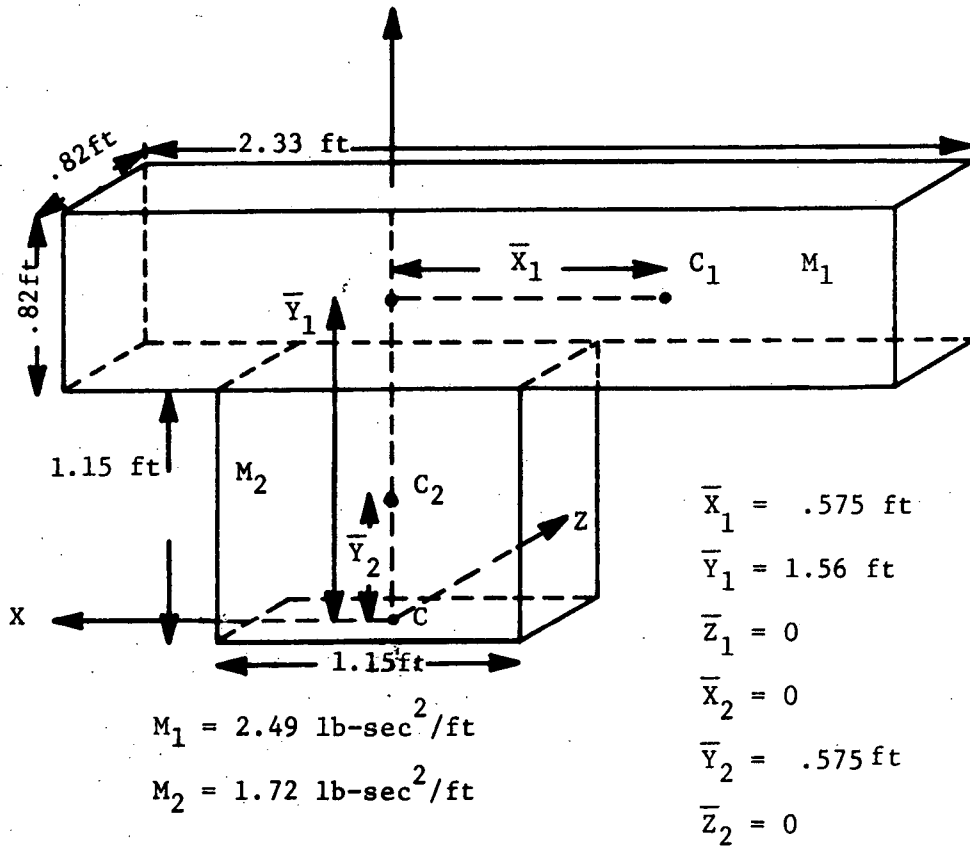


Figure V-1. Television Camera and Mount

$$[I] = \begin{bmatrix} I_{XX} & I_{XY} & 0 \\ I_{XY} & I_{YY} & 0 \\ 0 & 0 & I_{ZZ} \end{bmatrix} \quad (V-1)$$

where certain cross-product terms are zero since the XY plane is a plane of symmetry. The direction the TV camera points is described in terms of two Euler angles; first a rotation  $\psi_c$  about the Y axis and second a rotation  $\theta_c$  about the  $Z_c$  axis as is shown in Figure V-2.

Let  $w_1, w_2, w_3$  be the angular velocities of the TV camera about the  $x_c, y_c, z_c$  axes respectively. Then in matrix form the angular momentum vector is

$$[H]_{x_c y_c z_c} = \begin{bmatrix} I_{XX} & I_{XY} & 0 \\ I_{XY} & I_{YY} & 0 \\ 0 & 0 & I_{ZZ} \end{bmatrix} \begin{bmatrix} w_1 \\ w_2 \\ w_3 \end{bmatrix} \quad (V-2)$$

The torque vector is

$$[T]_{x_c y_c z_c} = \begin{bmatrix} T_1 \\ T_2 \\ T_3 \end{bmatrix} = \frac{d[H]_{x_c y_c z_c}}{dt} \quad (V-3)$$

Performing the indicated operation [5], [6] yields

$$\begin{bmatrix} T_1 \\ T_2 \\ T_3 \end{bmatrix} = \begin{bmatrix} I_{xx} \dot{w}_1 - I_{xy} \dot{w}_2 + I_{zz} w_2 w_3 + I_{xy} w_1 w_3 - I_{yy} w_2 w_3 \\ I_{xy} \dot{w}_2 - I_{xy} \dot{w}_1 - I_{zz} w_1 w_3 + I_{xx} w_1 w_3 - I_{xy} w_2 w_3 \\ I_{zz} \dot{w}_3 - I_{xy} w_1^2 + I_{yy} w_1 w_2 - I_{xx} w_1 w_2 + I_{xy} w_2^2 \end{bmatrix} \quad (V-4)$$

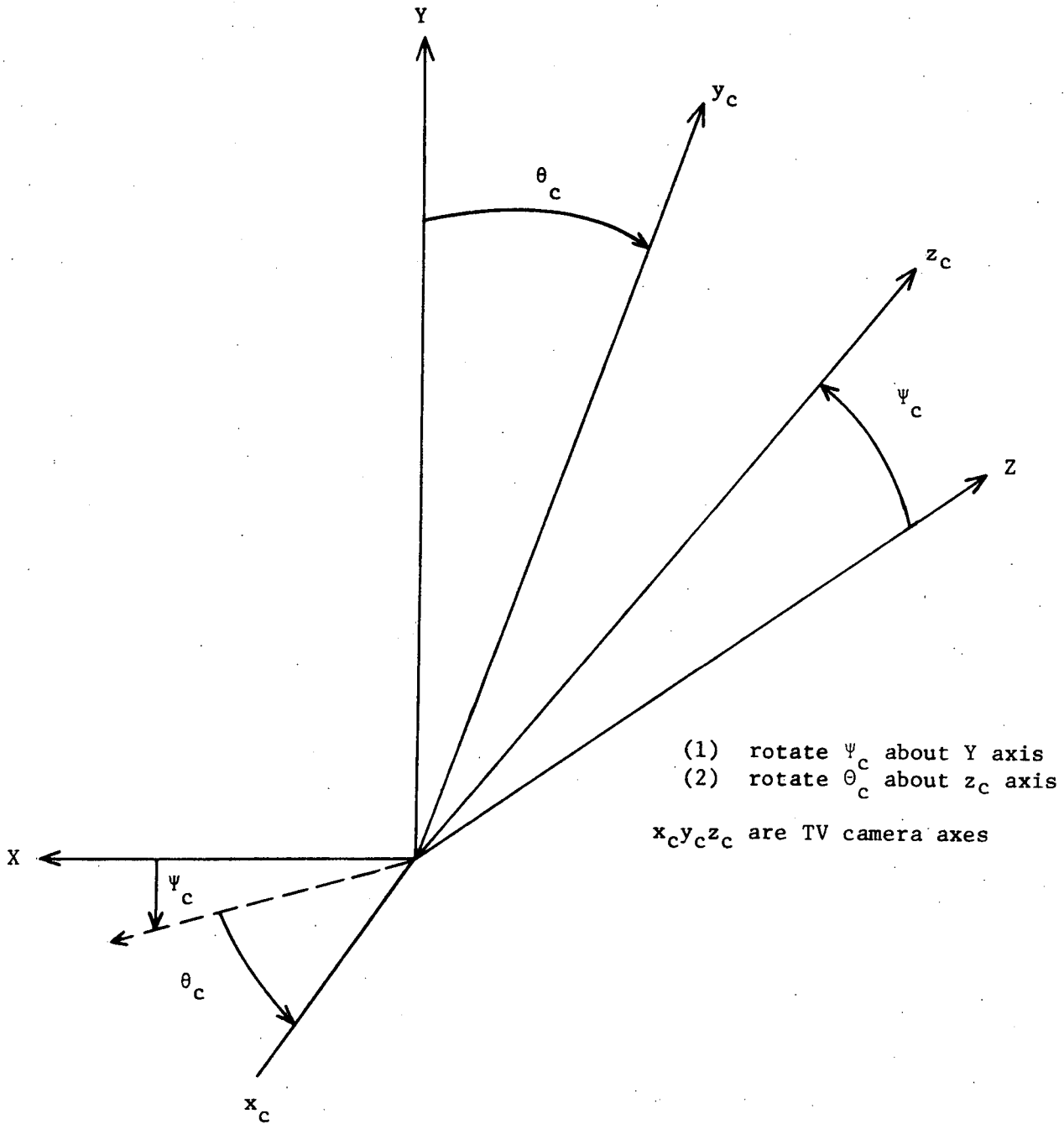


Figure V-2. Television Camera Coordinates

where

$$\begin{bmatrix} w_1 \\ w_2 \\ w_3 \end{bmatrix} = \begin{bmatrix} \dot{\psi}_c \sin \theta_c \\ \dot{\psi}_c \cos \theta_c \\ \dot{\theta}_c \end{bmatrix} \quad (V-5)$$

and

$$\begin{bmatrix} \dot{w}_1 \\ \dot{w}_2 \\ \dot{w}_3 \end{bmatrix} = \begin{bmatrix} \ddot{\psi}_c \sin \theta_c + \dot{\psi}_c \dot{\theta}_c \cos \theta_c \\ \ddot{\psi}_c \cos \theta_c - \dot{\psi}_c \dot{\theta}_c \sin \theta_c \\ \ddot{\theta}_c \end{bmatrix} \quad (V-6)$$

Let  $T_x$ ,  $T_y$ ,  $T_z$  be the torques about the XYZ axes. The transformation is

$$\begin{bmatrix} T_x \\ T_y \\ T_z \end{bmatrix} = \begin{bmatrix} \cos \psi_c \cos \theta_c & -\cos \psi_c \sin \theta_c & \sin \psi_c \\ \sin \theta_c & \cos \theta_c & 0 \\ -\sin \psi_c \cos \theta_c & \sin \psi_c \sin \theta_c & \cos \psi_c \end{bmatrix} \begin{bmatrix} T_1 \\ T_2 \\ T_3 \end{bmatrix} \quad (V-7)$$

Performing the indicated operations results in the following expressions for the disturbing torques about the spacecraft center-of-mass, written in terms of the TV camera and mount inertias and the Euler angles  $\theta_c$  and  $\psi_c$ :

$$\begin{aligned} T_x = & \left\{ \frac{I_{xx} - I_{yy}}{2} \sin 2\theta_c - I_{xy} \cos 2\theta_c \right\} (\cos \psi_c) \ddot{\psi}_c + \\ & \left\{ I_{zz} \sin \psi_c \right\} \ddot{\theta}_c + \\ & \{ (I_{xx} - I_{yy}) \cos 2\theta_c + I_{zz} + 2I_{xy} \sin 2\theta_c \} (\cos \psi_c) \dot{\psi}_c \dot{\theta}_c + \\ & \{ I_{xy} \cos 2\theta_c - \frac{(I_{xx} - I_{yy})}{2} \sin 2\theta_c \} (\sin \psi_c) \dot{\psi}_c^2 \end{aligned} \quad (V-8)$$

$$T_y = \{I_{xx} \sin^2 \theta_c + I_{yy} \cos^2 \theta_c - I_{xy} \sin 2\theta_c\} \ddot{\psi}_c + \\ \{(I_{xx} - I_{yy}) \sin 2\theta_c - 2I_{xy} \cos 2\theta_c\} \dot{\psi}_c \dot{\theta}_c \quad (V-9)$$

$$T_z = \{I_{xy} \cos 2\theta_c + \frac{(-I_{xx} + I_{yy}) \sin 2\theta_c}{2}\} (\sin \psi_c) \ddot{\psi}_c + \\ \{-2I_{xy} \sin 2\theta_c + I_{yy} \cos 2\theta_c - I_{xx} \cos 2\theta_c - I_{zz}\} (\sin \psi_c) \dot{\psi}_c \dot{\theta}_c \\ + I_{zz} (\cos \psi_c) \ddot{\theta}_c + \\ \left\{ \frac{-I_{xx} + I_{yy}}{2} \sin 2\theta_c + I_{xy} \cos 2\theta_c \right\} (\cos \psi_c) \dot{\psi}_c^2 \quad (V-10)$$

#### Part B. Computation of the Inertias for the TV Camera and Mount

The TV camera and mount are considered as two rectangular blocks with centers-of-mass at  $C_1$  and  $C_2$  respectively, as shown in Figure V-1. The equations to compute the inertias of rectangular blocks are well-known [6] and yield for  $M_1$ , about  $C_1$ ,

$$I_{x_1y_1} = \frac{M_1(b^2 + c^2)}{12} = .28 \text{ lb-ft-sec}^2$$

$$I_{y_1y_1} = \frac{M_1(a^2 + c^2)}{12} = 1.27 \text{ lb-ft-sec}^2$$

$$I_{z_1z_1} = \frac{M_1(a^2 + b^2)}{12} = 1.27 \text{ lb-ft-sec}^2$$

where  $M_1 = 2.49 \text{ lb-sec}^2/\text{ft}$

$$a = 2.33 \text{ ft}$$

$$b = 0.82 \text{ ft}$$

$$c = 0.82 \text{ ft}$$



For  $M_2$  about  $C_2$ ,

$$I_{x_2x_2} = \frac{M_2(b^2 + c^2)}{12} = 0.285 \text{ lb-ft-sec}^2$$

$$I_{y_2y_2} = \frac{M_2(c^2 + a^2)}{12} = 0.285 \text{ lb-ft-sec}^2$$

$$I_{z_2z_2} = \frac{M_2(a^2 + b^2)}{12} = 0.378 \text{ lb-ft-sec}^2$$

where

$$M_2 = 1.72 \text{ lb - sec}^2/\text{ft}$$

$$a = 1.15 \text{ ft}$$

$$b = 1.15 \text{ ft}$$

$$c = 0.82 \text{ ft}$$

The parallel-axis theorem [6] is used to compute the moments-of-inertias of the two bodies about C. This yields

$$I_{xx} = I_{x_1x_1} + I_{x_2x_2} + M_1 \bar{Y}_1^2 + M_2 \bar{Y}_2^2 = 7.193 \text{ lb-ft-sec}^2$$

$$I_{yy} = I_{y_1y_1} + I_{y_2y_2} + M_1 \bar{X}_1^2 = 2.34 \text{ lb-ft-sec}^2$$

$$I_{zz} = I_{z_1z_1} + I_{z_2z_2} + M_1 (\bar{Y}_1^2 + \bar{X}_1^2) + M_2 (\bar{Y}_2^2) = 9.05 \text{ lb-ft-sec}^2$$

The non-zero cross-product term is

$$I_{xy} = M_1 \bar{X}_1 \bar{Y}_1 = 2.22 \text{ lb-ft-sec}^2$$

where the values of  $\bar{X}_1$ ,  $\bar{Y}_1$ ,  $\bar{Y}_2$  are listed on Figure V-1.

### Part C. Computation of Disturbing Torques

The inertias computed in Part B are substituted in (V-8), (V-9), (V-10). The resulting equations are

$$\begin{aligned}
 T_x = & \{2.425 \sin 2\theta_c - 2.22 \cos 2\theta_c\}(\cos \psi_c)\ddot{\psi}_c + \\
 & 9.05 (\sin \psi_c)\ddot{\theta}_c + \\
 & \{4.85 \cos 2\theta_c + 9.05 + 4.44 \sin 2\theta_c\}(\cos \psi_c)\dot{\psi}_c\dot{\theta}_c + \\
 & \{2.22 \cos 2\theta_c - 2.425 \sin 2\theta_c\}(\sin \psi_c)\dot{\psi}_c^2
 \end{aligned} \tag{V-11}$$

$$\begin{aligned}
 T_y = & \{7.19 \sin^2 \theta_c + 2.34 \cos^2 \theta_c - 2.22 \sin 2\theta_c\}\ddot{\psi}_c + \\
 & \{4.85 \sin 2\theta_c - 4.44 \cos 2\theta_c\}\dot{\psi}_c\dot{\theta}_c
 \end{aligned} \tag{V-12}$$

$$\begin{aligned}
 T_z = & \{2.22 \cos 2\theta_c - 2.425 \sin 2\theta_c\}(\sin \psi_c)\ddot{\psi}_c + \\
 & 9.05 (\cos \psi_c)\ddot{\theta}_c + \\
 & \{-4.44 \sin 2\theta_c - 4.85 \cos 2\theta_c - 9.05\}(\sin \psi_c)\dot{\psi}_c\dot{\theta}_c + \\
 & \{-2.425 \sin 2\theta_c + 2.22 \cos 2\theta_c\}(\cos \psi_c)\dot{\psi}_c^2
 \end{aligned} \tag{V-13}$$

To obtain numerical values for the disturbing torques it is necessary to assume scanning rates and accelerations for the TV camera. It is assumed that these values are bounded by

$$-10^\circ/\text{sec} \leq \dot{\theta}_c, \dot{\psi}_c \leq +10^\circ/\text{sec} \quad (.174 \text{ rad/sec})$$

$$-10^\circ/\text{sec}^2 \leq \ddot{\theta}_c, \ddot{\psi}_c \leq +10^\circ/\text{sec}^2 \quad (.174 \text{ rad/sec}^2)$$

Interest is in those conditions which result in large disturbing torques.

The entries in Table 1, except for the one designated "upper bound" (but not least upper bound) were computed for selected values of  $\theta_c$  and  $\psi_c$  by assigning scanning rates and accelerations so all terms are of the same sign and thus additive.

The entry in Table 1 designated the "upper bound" was computed by maximizing (or minimizing) each term in (V-11) with respect to  $\theta_c$  and assigning the polarity of the scanning rates and accelerations so all terms are positive. Next  $\psi_c$  was determined by solving  $\frac{\partial T_x}{\partial \psi_c} = 0$ .

The following illustrates this procedure:

Referring to (V-11) let

$$f_1(\theta_c) = 2.425 \sin 2\theta_c - 2.22 \cos 2\theta_c$$

$$\frac{\partial f_1(\theta_c)}{\partial \theta_c} = 0 \text{ yields } \theta_c = -23.75^\circ \text{ and } f_1(-23.75^\circ) = 3.287$$

$$f_2(\theta_c) = 4.85 \cos 2\theta_c + 9.05 + 4.44 \sin 2\theta_c$$

$$\frac{\partial f_2(\theta_c)}{\partial \theta_c} = 0 \text{ yields } \theta_c = +21.25^\circ \text{ and } f_2(21.25^\circ) = 15.62$$

$$f_3(\theta_c) = 2.22 \cos 2\theta_c - 2.425 \sin 2\theta_c$$

$$\frac{\partial f_3(\theta_c)}{\partial \theta_c} = 0 \text{ yields } \theta_c = -23.75^\circ \text{ and } f_3(-23.75^\circ) = 3.287$$

Next the scanning rates and accelerations are chosen so all terms are positive. This yields

$$T_x = (3.287)(.174) \cos \psi_c + (9.05)(.174) \sin \psi_c + (15.62)(.174)^2 \sin \psi_c + (3.287)(.174)^2 \sin \psi_c \quad (\text{V-14})$$

Evaluating  $\frac{\partial T_x}{\partial \psi_c} = 0$  yields  $\psi_c = 58^\circ$ . This value gives

$$T_x = 1.97 \text{ lb-ft-sec}^2$$

upper bound

The disturbing torques computed are comparable in magnitude to the torques available from the RCJ thrusters which for comparison purposes are listed at the bottom of Table 1. The conclusion to be drawn is that for the dimensions, mass, and scanning rates and accelerations assumed, the disturbing torques are significant. Equations (V-8), (V-9), (V-10) and the procedure outlined for computing an upper bound on the disturbing torque can be used to study the effect of changes in the parameters of the TV camera and mount.

$T_x$  Calculations

$\theta_c$ deg	$\psi_c$ deg	$\dot{\theta}_c$ deg/sec	$\dot{\psi}_c$ deg/sec	$\ddot{\theta}_c$ deg/sec <sup>2</sup>	$\ddot{\psi}_c$ deg/sec <sup>2</sup>	Torque lb-ft
-23.75	20	10	10	0	0	.2900
21.25	0	10	10	0	0	.469
45.0	0	10	10	0	0	.3021
21.25	18.6	10	10	10	10	.9477
-23.75	81	10	10	10	0	1.6953
0	63.9	10	10	10	-10	1.8294
-23.75	63.9	10	10	10	-10	1.8742
---	58	10	10	10	-10	1.97*
$T_y$ Calculations						
11.65	---	10	10	---	10	.223
21.25	---	---	0	---	10	.2595
-30.85	---	10	10	---	10	1.16125
$T_z$ Calculations						
21.25	90	10	10	0	10	.4729
-23.75	26.8	-10	10	10	10	1.87688

\* Upper-bound

note: RCJ torques are:

$$T_x = 1.8 \text{ lb-ft}$$

$$T_y = 1.28 \text{ lb-ft}$$

$$T_z = 1.28 \text{ lb-ft}$$

Table 1. Disturbing Torques due to Motion of Television Camera

## VI. CONCLUSIONS AND RECOMMENDATIONS

One objective of this study was to design a highly reliable attitude control system for experiment pointing, station keeping, docking and separation from the target for the CARD space vehicle. The design presented herein is based on using a RCJ attitude control system and/or a CMG attitude control system. The combined system was designed so that the torques from each system are never in opposition and to minimize cross-coupling of the axes.

The RCJ attitude control system uses a no-fire region similar to that employed on the Skylab program [2]. A modification was introduced which results in more predictable phase-plane trajectories for the Y-axis and Z-axis control systems and shows promise of improved performance. In essence, in place of controlling  $\phi_y$  and  $\phi_z$ , the Y-axis attitude and Z-axis attitude respectively, the feedbacks are arranged so that  $(\phi_z + \phi_y)$  and  $(\phi_z - \phi_y)$  are being controlled. If the phase-plane trajectories are plotted as  $(A_{1z}\dot{\phi}_z + A_{1y}\dot{\phi}_y)$  vs  $(\phi_z + \phi_y)$  and  $(A_{1z}\dot{\phi}_z - A_{1y}\dot{\phi}_y)$  vs  $(\phi_z - \phi_y)$  rather than  $\dot{\phi}_z$  vs  $\phi_z$  and  $\dot{\phi}_y$  vs  $\phi_y$  then the trajectories can be superimposed on the no-fire boundaries. More test runs need to be made to evaluate this system.

The CMG system simulated for this study uses the optimum steering law described in [4]. This steering law was chosen for convenience; the approach to designing the system was general and could have employed

any steering law. The state-space analysis of the CMG system led to the required structure of the input matrix (steering law) and of the feedback matrix if the system axes are to be decoupled. The optimum steering law and proportional-plus-rate feedback are shown to be special cases. Additional work is needed to determine if this approach will lead to better steering laws and feedback schemes.

In the attitude control system using both the CMG's and the RCJ's the feedback for the Y-axis and the Z-axis are the sum and difference signals. The torque reversal line of the CMG system was designed to be in the middle of the RCJ system no-fire region. With this design the two systems never produce opposing torques. Additional phase-plane trajectories are needed to fully evaluate this system and other CMG torque reversal lines need to be investigated.

Another objective of this study was to derive a procedure for computing the disturbing torques due to the motion of the on-board TV camera. The equations for the torques in terms of the TV camera and mount inertias and scanning rates and accelerations were derived. A simplified procedure for computing the upper bound (but not the least upper bound) of the torques was outlined. More precise computations can be made once the camera requirements are better defined.

#### REFERENCES

- [1]. "A Feasibility Study of Unmanned Comet and Asteroid Rendezvous and Docking Concepts Using Solar Electric Propulsion (CARD)" Vol. II, Concept Analysis, Planning and Cost, Final Report under Contract NAS8-27206, Northrup Services, Inc., October, 1971.
- [2]. A. C. McCullough, C. C. Rupp, "Skylab Nested Attitude Control System Concept", Proceedings of the ION National Space Meeting on the Space Shuttle, Space Station, Nuclear Shuttle Navigation, February 23-25, 1971.
- [3]. D. W. Russell et.al., "Study of Limit Cycle Behavior For An On-Off Attitude Control System Using Linear Signal Mixing", Twelfth Technical Report, Contract NAS8-2484, Auburn Research Foundation, October, 1964.
- [4]. J. S. Boland, III., et.al., "Study of an Improved Attitude Control System", Twenty-fifth Technical Report, Contract NAS8-20104, Auburn University, December, 1970.
- [5]. D. A. Wells, "Theory and Problems of Lagrangian Dynamics", Schaum Outline Series, McGraw-Hill Book Company, 1967.
- [6]. H. Goldstein, "Classical Mechanics", Addison-Wesley, 1950.



APPENDIX ATTITUDE CONTROL SYSTEM SIMULATION PROGRAM

RCJ Attitude Control System - Linear Signal Mixing - Sum and Difference Feedback

and/or

CMG Attitude Control System - Optimum Steering Law - Sum and Difference Feedback

Input Data

DELT	Integration step size, seconds
PRDEL	Print increment, seconds
FINTIM	Total simulation time
INERTX	x-axis moment-of-inertia, lb-ft-sec <sup>2</sup>
INERTY	y-axis moment-of-inertia, lb-ft-sec <sup>2</sup>
CUTOFF	Minimum absolute value of det [A]
GSTOP	Gimbal stop, radians
FPX	x-axis position feedback gain
FPY	y-axis position feedback gain
FPZ	z-axis position feedback gain
AMX	x-axis acceleration due to RCJ thrusters deg/sec
AMY	y-axis acceleration due to RCJ thrusters deg/sec
AMZ	z-axis acceleration due to RCJ thrusters deg/sec.
RLDGX	x-axis rate ledge, deg/sec

RLDGY	y-axis rate ledge, deg/sec
RLDGZ	z-axis rate ledge, deg/sec
PDB	Deadband, deg
TQMTRL	Torque motor rate limit, rad/sec
PHIX	Initial value of x-axis angle, deg
PHIY	Initial value of y-axis angle, deg
PHIZ	Initial value of z-axis angle, deg
DPX	Initial value of x-axis rate, deg/sec
DPY	Initial value of y-axis rate, deg/sec
DPZ	Initial value of z-axis rate, deg/sec
DEL 11	Initial value of $\delta_{11}$ , deg
DEL 12	Initial value of $\delta_{12}$ , deg
DEL 13	Initial value of $\delta_{13}$ , deg
DEL 31	Clamped value of $\delta_{31}$ , deg
DEL 32	Clamped value of $\delta_{32}$ , deg
DEL 33	Clamped value of $\delta_{33}$ , deg

```

REAL MXCMND,MYCMND,MZCMND,MXCMDE,MYCMDE,MZCMDE,MRX,MRY,MRZ,MTRXC,
$   INERTX,INERTY,INERTZ,M1,M2,M3,M1INT,M2INT,M3INT
COMMON RDIAN,INERTX,INERTY,INERTZ,FPX,FPY,FPZ,FDPX,FDPY,FCPZ
COMMON/B1/DLDT11,DLDT12,DLDT13,MXCMND,MXCMDE,MRX,MRY,MRZ,MTRXD,
$   CDT11C,CDT12C,CDT13C,DEL31R,DEL32R,DEL33R,CUTOFF,GSTOP,
$   EX,EY,EZ,DDPXT,DDPYT,DDPZT,TRXV,TRYV,TRZV
COMMON/B4/AIX,AIY,AIZ,PRX,PRY,PRZ
DELT =0.02
PRDEL =0.2
FINTIM=60.
INERTX=1127.
INERTY=2947.
INERTZ=2918.
CUTOFF=.05
GSTOP=3.
FPX=700.
FPY=1000.
FPZ=1000.
AMX=.208
AMY=.0391
AMZ=.0378
RLDGX=.172
RLDGY=.172
RLDGZ=.172
PDB=.3
X1=4.*PDB*AMX+RLDGX**2
Y1=4.*PDB*AMY+RLDGY**2
Z1=4.*PDB*AMZ+RLDGZ**2
X2=8.*AMX*(2.*AMX*PDB**2-PDB*RLDGX**2)
Y2=8.*AMY*(2.*AMY*PDB**2-PDB*RLDGY**2)
Z2=8.*AMZ*(2.*AMZ*PDB**2-PDB*RLDGZ**2)
PRX=(X1+SQRT(X1**2-X2))/(4.*AMX)
PRY=(Y1+SQRT(Y1**2-Y2))/(4.*AMY)
PRZ=(Z1+SQRT(Z1**2-Z2))/(4.*AMZ)
AIX=SQRT((PRX+PDB)/(2.*AMX))
AIY=SQRT((PRY+PDB)/(2.*AMY))
AIZ=SQRT((PRZ+PDB)/(2.*AMZ))
WRITE(6,20)AIX,AIY,AIZ
WRITE(6,30)PRX,PRY,PRZ
20 FORMAT('1','AIX  =',E13.5,4X,'AIY  =',E13.5,4X,'AIZ  =',E13.5/)
30 FORMAT(' ','PRX  =',E13.5,4X,'PRY  =',E13.5,4X,'PRZ  =',E13.5////)
PHIX=5.
PHIY=0.
PHIZ=0.
DPX =0.
DPY =0.
DPZ =0.
DEL11=0.

```

```

DEL12=0.
DEL13=C.
M1INT=0.
M2INT=C.
M3INT=0.
DEL31=45.
DEL32=45.
DEL33=45.
RADIAN=57.29578
DEL11R=DEL11/RADIAN
DEL12R=DEL12/RADIAN
DEL13R=DEL13/RADIAN
DEL31R=DEL31/RADIAN
DEL32R=DEL32/RADIAN
DEL33R=DEL33/RADIAN
TEST=-DELT/2.
TIME=C.0
FUEL=C.
DO 900 I=1,100000
IF(TIME.GT.FINTIM)GO TO 1000
CALL      FCN(TIME,PHIX,DPX,PHIY,DPY,PHIZ,DPZ,
$          DEL11R,DEL12R,DEL13R,M1INT,M2INT,M3INT,
$          FCN1,FCN2,FCN3,FCN4,FCN5,FCN6,
$          FCN7,FCN8,FCN9,FCN10,FCN11,FCN12)
SUM=PHIY+PHIZ
DIFF=PHIY-PHIZ
DSUM=A1Y*DPY+A1Z*DPZ
DDIFF=A1Y*DPY-A1Z*DPZ
DDPXT=0.
DDPYT=0.
DDPZT=0.
FUELA=0.
IF(ABS(EX).LT.PDB) GO TO 100
CDPXT=CDPXT+SIGN(AMX,EX)
FUELA=FUELA+4.*DELT
100 IF(ABS(EY).LT.PDB) GO TO 110
CDPYT=CDPYT+.5*SIGN(AMY,EY)
CDPZT=CDPZT+.5*SIGN(AMZ,EY)
FUELA=FUELA+2.*DELT
110 IF(ABS(EZ).LT.PDB) GO TO 120
DDPYT=DDPYT-.5*SIGN(AMY,EZ)
CDPZT=CDPZT+.5*SIGN(AMZ,EZ)
FUELA=FUELA+2.*DELT
120 CONTINUE
AB11=ABS(DEL11R)
AB12=ABS(DEL12R)
AB13=ABS(DEL13R)
IF(AB11.GE.GSTOP.OR.AB12.GE.GSTOP.OR.AB13.GE.GSTOP)GO TO 910

```

```

IF (ABS(CDPXT).GT.AMX/4.0) GO TO 300
IF (ABS(CDPYT).GT.AMY/4.0) GO TO 300
IF (ABS(CDPZT).GT.AMZ/4.0) GO TO 300
IF (TIME.LT.TEST) GO TO 400
TEST=TEST+PRDEL
GO TO 310
300 CONTINUE
PRODX=CDPXT*MRX
PRODY=CDPYT*MRY
PRCDZ=CDPZT*MRZ
IF (PRCDX.LT.C.) WRITE(6,197)
IF (PRCDY.LT.O.) WRITE(6,198)
IF (PRCDZ.LT.C.) WRITE(6,199)
197 FORMAT(' ', '***X-AXIS GAS THRUSTERS OPPOSE CMGS***')
198 FORMAT(' ', '***Y-AXIS GAS THRUSTERS OPPOSE CMGS***')
199 FORMAT(' ', '***Z-AXIS GAS THRUSTERS OPPOSE CMGS***')
310 WRITE(6,200)TIME,PHIX,TRXV,CDPXT,DPX
WRITE(6,201)PHIY,TRYV,CDPYT,DPY
WRITE(6,202)PHIZ,TRZV,CDPZT,DPZ
WRITE(6,203)DEL11,DEL12,DEL13,MTRXD
WRITE(6,204)SUM,DSUM,DIFF,DDIFF
WRITE(6,205)FUEL
400 FUEL=FUEL+FUELA
CALL INTGRL(TIME,DELT,FCN1,FCN2,FCN3,FCN4,FCN5,FCN6,
$          FCN7,FCN8,FCN9,FCN10,FCN11,FCN12,
$          PHIX,CPX,PHIY,DPY,PHIZ,DPZ,
$          DEL11R,DEL12R,DEL13R,M1INT,M2INT,M3INT)
DEL11=DEL11R*RADIAN
DEL12=DEL12R*RADIAN
DEL13=DEL13R*RADIAN
TIME=TIME+DELT
900 CONTINUE
GO TO 1000
910 WRITE(6,920)
920 FORMAT(' ', '***GIMBAL ANGLE EXCEEDS GIMBAL STOP***')
WRITE(6,200)TIME,PHIX,TRXV,CDPXT,DPX
WRITE(6,201)PHIY,TRYV,CDPYT,DPY
WRITE(6,202)PHIZ,TRZV,CDPZT,DPZ
WRITE(6,204)SUM,DSUM,DIFF,DDIFF
WRITE(6,203)DEL11,DEL12,DEL13,MTRXD
WRITE(6,205)FUEL
200 FORMAT(' ', 'TIME =',E12.4,5X,'PHIX =',E13.5,5X,'TRXV =',E13.5,
$          5X,'CDPXT =',E13.5,5X,'DPX =',E13.5)
201 FORMAT(25X,'PHIY =',E13.5,5X,'TRYV =',E13.5,5X,'DDPYT =',E13.5,
$          5X,'DPY =',E13.5)
202 FORMAT(25X,'PHIZ =',E13.5,5X,'TRZV =',E13.5,5X,'DDPZT =',E13.5,
$          5X,'DPZ =',E13.5)
203 FORMAT(25X,'DEL11 =',E13.5,5X,'DEL12 =',E13.5,5X,'DEL13 =',E13.5,

```

```

$          5X,'MTRXD =' ,E13.5)
204 FORMAT(25X,'SUM   =' ,E13.5,5X,'DSUM  =' ,E13.5,5X,'DIFF  =' ,E13.5,
$          5X,'CDIFF =' ,E13.5)
205 FORMAT(25X,'FUEL  =' ,E13.5/)
1000 STOP
      END
```

```

SUBROUTINE INTGRL(T,H,FCN1,FCN2,FCN3,FCN4,FCN5,FCN6,
$      FCN7,FCN8,FCN9,FCN10,FCN11,FCN12,Y1,Y2,Y3,Y4,Y5,Y6,
$      Y7,Y8,Y9,Y10,Y11,Y12)
H2=H/2.
CALL FCN(T,Y1,Y2,Y3,Y4,Y5,Y6,Y7,Y8,Y9,Y10,Y11,Y12,FCN1,FCN2,FCN3,
$      FCN4,FCN5,FCN6,FCN7,FCN8,FCN9,FCN10,FCN11,FCN12)
P1=H*FCN1
P2=H*FCN2
P3=H*FCN3
P4=H*FCN4
P5=H*FCN5
P6=H*FCN6
P7=H*FCN7
P8=H*FCN8
P9=H*FCN9
P10=H*FCN10
P11=H*FCN11
P12=H*FCN12
CALL FCN(T+H2,Y1+P1/2.,Y2+P2/2.,Y3+P3/2.,Y4+P4/2.,Y5+P5/2.,
$      Y6+P6/2.,Y7+P7/2.,Y8+P8/2.,Y9+P9/2.,Y10+P10/2.,Y11+P11/2.,
$      Y12+P12/2.,FCN1,FCN2,FCN3,FCN4,FCN5,FCN6,FCN7,FCN8,FCN9,
$      FCN10,FCN11,FCN12)
Q1=H*FCN1
Q2=H*FCN2
Q3=H*FCN3
Q4=H*FCN4
Q5=H*FCN5
Q6=H*FCN6
Q7=H*FCN7
Q8=H*FCN8
Q9=H*FCN9
Q10=H*FCN10
Q11=H*FCN11
Q12=H*FCN12
CALL FCN(T+H2,Y1+Q1/2.,Y2+Q2/2.,Y3+Q3/2.,Y4+Q4/2.,Y5+Q5/2.,
$      Y6+Q6/2.,Y7+Q7/2.,Y8+Q8/2.,Y9+Q9/2.,Y10+Q10/2.,Y11+Q11/2.,
$      Y12+Q12/2.,FCN1,FCN2,FCN3,FCN4,FCN5,FCN6,FCN7,FCN8,FCN9,
$      FCN10,FCN11,FCN12)
R1=H*FCN1
R2=H*FCN2
R3=H*FCN3
R4=H*FCN4
R5=H*FCN5
R6=H*FCN6
R7=H*FCN7
R8=H*FCN8
R9=H*FCN9
R10=H*FCN10

```

```
R11=H*FCN11
R12=H*FCN12
CALL FCN(I+H,Y1+R1,Y2+R2,Y3+R3,Y4+R4,Y5+R5,Y6+R6,Y7+R7,Y8+R8,
$      Y9+R9,Y10+R10,Y11+R11,Y12+R12,FCN1,FCN2,FCN3,FCN4,FCN5,FCN6,
$      FCN7,FCN8,FCN9,FCN10,FCN11,FCN12)
S1=H*FCN1
S2=H*FCN2
S3=H*FCN3
S4=H*FCN4
S5=H*FCN5
S6=H*FCN6
S7=H*FCN7
S8=H*FCN8
S9=H*FCN9
S10=H*FCN10
S11=H*FCN11
S12=H*FCN12
Y1=Y1+(P1+2.*(Q1+R1)+S1)/6.
Y2=Y2+(P2+2.*(Q2+R2)+S2)/6.
Y3=Y3+(P3+2.*(Q3+R3)+S3)/6.
Y4=Y4+(P4+2.*(Q4+R4)+S4)/6.
Y5=Y5+(P5+2.*(Q5+R5)+S5)/6.
Y6=Y6+(P6+2.*(Q6+R6)+S6)/6.
Y7=Y7+(P7+2.*(Q7+R7)+S7)/6.
Y8=Y8+(P8+2.*(Q8+R8)+S8)/6.
Y9=Y9+(P9+2.*(Q9+R9)+S9)/6.
Y10=Y10+(P10+2.*(Q10+R10)+S10)/6.
Y11=Y11+(P11+2.*(Q11+R11)+S11)/6.
Y12=Y12+(P12+2.*(Q12+R12)+S12)/6.
RETURN
END
```



```

SUBROUTINE FCN(TIME,PHIX,DPX,PHIY,DPY,PHIZ,DPZ,
$           DEL11R,DEL12R,DEL13R,M1INT,M2INT,M3INT,
$           FCN1,FCN2,FCN3,FCN4,FCN5,FCN6,FCN7,FCN8,
$           FCN9,FCN10,FCN11,FCN12)
REAL MXCMND,MYCMND,MZCMND,MXCMDE,MYCMDE,MZCMDE,MRX,MRY,MRZ,MTRXD,
$     INERTX,INERTY,INERTZ,M1,M2,M3,M1INT,M2INT,M3INT
COMMON RACIAN,INERTX,INERTY,INERTZ,FPX,FPY,FPZ,FDPX,FDPY,FDPZ
COMMON/B1/DLOT11,DLOT12,DLOT13,MXCMND,MXCMDE,MRX,MRY,MRZ,MTRXD,
$     DDT11C,DDT12C,DDT13C,DEL31R,DEL32R,DEL33R,CUTOFF,GSTOP,
$     EX,EY,EZ,DDPXT,DDPYT,DDPZT,TRXV,TRYV,TRZV
COMMON/B4/A1X,A1Y,A1Z,PRX,PRY,PRZ
A11= SIN(DEL11R)*CCS(DEL31R)
A12= CCS(DEL12R)
A13=-SIN(DEL13R)*SIN(DEL33R)
A21=-SIN(DEL11R)*SIN(DEL31R)
A22= SIN(DEL12R)*COS(DEL32R)
A23= CCS(DEL13R)
A31= CCS(DEL11R)
A32=-SIN(DEL12R)*SIN(DEL32R)
A33= SIN(DEL13R)*COS(DEL33R)
MTRXD= A11*A22*A33+A12*A23*A31+A21*A32*A13
$     -A13*A22*A31-A12*A21*A33-A23*A32*A11
IF(ABS(MTRXD).LT.CUTOFF)MTRXD=SIGN(CUTOFF,MTRXD)
T11=( A22*A33-A23*A32)/MTRXD
T12=(-A12*A33+A13*A32)/MTRXD
T13=( A12*A23-A13*A22)/MTRXD
T21=(-A21*A33+A23*A31)/MTRXD
T22=( A11*A33-A13*A31)/MTRXD
T23=(-A11*A23+A13*A21)/MTRXD
T31=( A21*A32-A22*A31)/MTRXD
T32=(-A11*A32+A12*A31)/MTRXD
T33=( A11*A22-A12*A21)/MTRXD
DDT11R=5.*M1INT
DDT12R=5.*M2INT
DDT13R=5.*M3INT
DLCT11=DDT11R*RADIAN
DLCT12=DDT12R*RADIAN
DLCT13=DDT13R*RADIAN
PXF=PHIX
PYF=PHIY+PHIZ
PZF=PHIZ-PHIY
IF(ABS(PXF).GT.PRX) PXF=SIGN(PRX,PXF)
IF(ABS(PYF).GT.PRY) PYF=SIGN(PRY,PYF)
IF(ABS(PZF).GT.PRZ) PZF=SIGN(PRZ,PZF)
EX=- (A1X*DPX+PXF)
EY=- (A1Z*DPZ+A1Y*DPY+PYF)
EZ=- (A1Z*DPZ-A1Y*DPY+PZF)
MXCMNC=FPX*EX/RADIAN

```

```
MYCMND=FPY*(EY-EZ)/RADIAN
MZCMND=FPZ*(EY+EZ)/RADIAN
MRX=(A11*DDT11R+A12*DDT12R+A13*DDT13R)*60.
MKY=(A21*DDT11R+A22*DDT12R+A23*DDT13R)*60.
MRZ=(A31*DDT11R+A32*DDT12R+A33*DDT13R)*60.
TRXV=RADIAN*MRX/INERTX
TRYV=RADIAN*MRY/INERTY
TRZV=RADIAN*MRZ/INERTZ
MXCMDE=MXCMND-MRX
MYCMDE=MYCMND-MRY
MZCMDE=MZCMND-MRZ
DDT11C=(T11*MXCMDE+T12*MYCMDE+T13*MZCMDE)/60.
DDT12C=(T21*MXCMDE+T22*MYCMDE+T23*MZCMDE)/60.
DDT13C=(T31*MXCMDE+T32*MYCMDE+T33*MZCMDE)/60.
DDT11G=2.*DDT11C
DDT12G=2.*DDT12C
DDT13G=2.*DDT13C
TQMTRL=4.5/RADIAN
IF(ABS(DDT11G).GT.TQMTRL)DDT11G=SIGN(TQMTRL,DDT11G)
IF(ABS(DDT12G).GT.TQMTRL)DDT12G=SIGN(TQMTRL,DDT12G)
IF(ABS(DDT13G).GT.TQMTRL)DDT13G=SIGN(TQMTRL,DDT13G)
FCN1=CPX
FCN2=TRXV+DDPXT
FCN3=CPY
FCN4=TRYV+DDPYT
FCN5=CPZ
FCN6=TRZV+DDPZT
FCN7=DDT11R
FCN8=DDT12R
FCN9=DDT13R
FCN10=DDT11G-DDT11R
FCN11=DDT12G-DDT12R
FCN12=DDT13G-DDT13R
RETURN
END
```